Equilibrated gas and carbonate standard-derived paired clumped isotope (Δ_{47} and Δ_{48}) values on the absolute reference frame

Journal:	*Rapid Communications in Mass Spectrometry*
Manuscript ID	RCM-21-0141.R1
Wiley - Manuscript type:	Research Article
Date Submitted by the Author:	n/a

Complete List of Authors:	Lucarelli, Jamie; University of California Los Angeles, Earth, Planetary & Space Sciences Carroll, Hannah; University of California Los Angeles, Department of Earth, Planetary, and Space Sciences, Department of Atmospheric and Oceanic Sciences, Institute of the Environment and Sustainability, Center for Diverse Leadership in Science Elliott, Ben; University of California Los Angeles, Earth, Planetary & Space Sciences Coplen, Tyler; U.S. Geological Survey, Eagle, Robert; University of California Los Angeles Tripati, Aradhna; University of California Los Angeles, Department of Earth, Planetary, and Space Sciences; Department of Atmospheric and Oceanic Sciences; Institute for the Environment and Sustainability; California Nanosystems Institute

Keywords:	clumped isotopes, Δ47, Δ48, paleoclimate, Devils Hole, Standards

Abstract:	Rationale: Carbonate clumped isotope geochemistry has focused on mass spectrometric determination of m/z 47 CO2 for geothermometry, but theory and experiments indicate paired analysis of the m/z 47 (13C-18O-16O) and m/z 48 (12C-18O-18O) isotopologues (denoted with Δ47 and Δ48 notation) can be used to study non-equilibrium isotope fractionations and refine temperature estimates. We utilize paired Δ47 and Δ48 measurements from a multi-year and multi-instrument dataset to constrain values for standards, study the equilibrium Δ47-Δ48 relationship, explore compositionally dependent acid digestion fractionation factors, and evaluate robust statistical analysis for replicate-level data. Methods: We determined Δ47 and Δ48 values of 27 carbonates using isotope-ratio mass spectrometry from 2015-2021. A total of 5,461 Δ47 and 3,400 Δ48 measurements of carbonates, and 183 Δ47 and 195 Δ48 measurements of gases are used from robust correction intervals for multiple instruments. Results: Equilibrated gas-based Δ47 and Δ48 values were determined for 7 carbonate standards. Carbonate-based standardization was used to determine Δ47 and Δ48 values for 27 carbonates, including standards and Devils Hole calcite. We provide constraints on the equilibrium Δ47-Δ48 relationship using theory and experimental regressions. We

demonstrate regression-form acid digestion fractionation factors (Δ*63-47 and Δ*64-48) agree with experimental data. A kernel density-based statistical method for data quality assurance is reported.
Conclusions: We demonstrate that as with Δ47, carbonate-based standardization can produce statistically indistinguishable Δ48 values across multiple instruments using different acid digestion methods and temperatures. Therefore, interlaboratory use of robustly determined Δ48 values for carbonate-based standardization should increase reproducibility. The experimental Δ47-Δ48 regressions reported here are statistically indistinguishable from recently published regressions from 0-600 oC. Data support published theoretical calculations that indicate acid digestion fractionation factors (Δ*63-47 and Δ*64-48) exhibit a subtle compositional dependence on the clumped isotope composition of carbonate minerals (Δ63 and Δ64). Statistically robust quality assurance methods adapted from other fields are applicable to clumped isotope data.

Equilibrated gas and carbonate standard-derived paired clumped isotope (Δ_{47} and Δ_{48}) values on the absolute reference frame

Rapid Communications in Mass Spectrometry

Jamie K. Lucarelli[1], Hannah M. Carroll[1], Ben M. Elliott[1], Tyler B. Coplen[2], Robert A. Eagle[1], Aradhna Tripati[1]

[1]Department of Earth, Planetary, and Space Sciences, Department of Atmospheric and Oceanic Sciences, Institute of the Environment and Sustainability, Center for Diverse Leadership in Science, UCLA, Los Angeles, CA 90095 USA.

[2]US Geological Survey, 12201 Sunrise Valley Drive, Reston, VA, 20192, USA

Correspondence to: jklucarelli@gmail.com and atripati@g.ucla.edu

Running Head: Robust Methods for Paired Carbonate Clumped Isotope Analysis (Δ_{47} and Δ_{48}) via IRMS

Rationale: Carbonate clumped isotope geochemistry has focused on mass spectrometric determination of *m/z* 47 CO_2 for geothermometry, but theory and experiments indicate paired analysis of the *m/z* 47 (^{13}C-^{18}O-^{16}O) and *m/z* 48 (^{12}C-^{18}O-^{18}O) isotopologues (denoted with Δ_{47} and Δ_{48} notation) can be used to study non-equilibrium isotope fractionations and refine temperature estimates. We utilize paired Δ_{47} and Δ_{48} measurements from a multi-year and multi-instrument dataset to constrain values for standards, study the equilibrium Δ_{47}-Δ_{48} relationship, explore compositionally dependent acid digestion fractionation factors, and evaluate robust statistical analysis for replicate-level data.

Methods: We determined Δ_{47} and Δ_{48} values of 27 carbonates using isotope-ratio mass spectrometry from 2015-2021. A total of 5,461 Δ_{47} and 3,400 Δ_{48} measurements of carbonates, and 183 Δ_{47} and 195 Δ_{48} measurements of gases are used from robust correction intervals for multiple instruments.

Results: Equilibrated gas-based Δ_{47} and Δ_{48} values were determined for 7 carbonate standards. Carbonate-based standardization was used to determine Δ_{47} and Δ_{48} values for 27 carbonates, including standards and Devils Hole calcite. We provide constraints on the equilibrium Δ_{47}-Δ_{48} relationship using theory and experimental regressions. We demonstrate regression-form acid digestion fractionation factors ($\Delta^*_{63\text{-}47}$ and $\Delta^*_{64\text{-}48}$) agree with experimental data. A kernel density-based statistical method for data quality assurance is reported.

Conclusions: We demonstrate that as with Δ_{47}, carbonate-based standardization can produce statistically indistinguishable Δ_{48} values across multiple instruments using different acid digestion methods and temperatures. Therefore, interlaboratory use of robustly determined Δ_{48} values for carbonate-based standardization should increase reproducibility. The experimental Δ_{47}-Δ_{48} regressions reported here are statistically indistinguishable from recently published

regressions from 0-600 °C. Data support published theoretical calculations that indicate acid digestion fractionation factors ($\Delta^*_{63\text{-}47}$ and $\Delta^*_{64\text{-}48}$) exhibit a subtle compositional dependence on the clumped isotope composition of carbonate minerals (Δ_{63} and Δ_{64}). Statistically robust quality assurance methods adapted from other fields are applicable to clumped isotope data.

INTRODUCTION

Equilibrium constants for internal isotope exchange reactions in $CaCO_3$ are directly related to mineral formation temperature.[1,2] This relationship is the basis for carbonate clumped isotope thermometry, which uses isotope ratio mass spectrometry to measure the frequency with which rare, heavy isotopes in carbonate minerals are bonded to each other (instead of bonded to much more common light isotopes) relative to a stochastic distribution. Historically, carbonate clumped isotope research has focused on carbonate ion groups with *m/z* of 63, which yields *m/z* 47 CO_2 after acid digestion.[2] Theory predicted that *m/z* 48 CO_2 isotopologues derived from acid digestion of *m/z* 64 $CaCO_3$ isotopologues in equilibrium precipitates could also be used for geothermometry.[2–6]

The unique attributes of carbonate clumped isotope thermometry based on determinations of *m/z* 47 CO_2 isotopologues and/or *m/z* 48 CO_2 isotopologues is that it does not depend on the bulk oxygen isotope composition (□^{18}O) of the water,[2] unlike the more widely used oxygen isotope thermometer[15]. Δ_{47} measurements have been used for the reconstruction of numerous paleo-environmental parameters, including but not limited to land[16] and ocean paleotemperatures[17,18], paleoelevation[19,20], and dinosaur body temperature[21], while simultaneously estimating water □^{18}O. However, previous research has shown that kinetic isotope effects observed in *m/z* 47 measurements of abiotic and biogenic carbonates, including speleothems[20,23] and coral[2,12,25,26] may affect the accuracy of temperature reconstructions.

While paired measurements of *m/z* 47 and 48 CO_2 can be used to probe equilibrium and kinetic isotope effects[5], due to their low abundance, measurements of *m/z* 48 isotopologues were used only to screen for contaminants prior to 2019[7]. The most abundant *m/z* 48 CO_2 isotopologue ($^{12}C^{18}O^{18}O$) has two ^{18}O substitutions and is therefore in extremely low abundance at 4.1 ppm in air, which is an order of magnitude lower than *m/z* 47 isotopologues (45 ppm).[2] The minor *m/z* 48 CO_2 isotopologue ($^{13}C^{18}O^{17}O$) has an abundance of 16.7 ppb.[2] The abundance of the dominant *m/z* 47 and *m/z* 48 CO_2 isotopologues, $^{13}C\text{-}^{18}O\text{-}^{16}O$ and $^{12}C\text{-}^{18}O\text{-}^{18}O$ isotopologues, is denoted with Δ_{47} and Δ_{48} notation.[8] These are defined as:

$$\Delta_{47} = [(R47\text{sample}/R47\text{stochastic} - 1) \qquad \text{Equation 1}$$

$$\Delta_{48} = (R48\text{sample}/R48\text{stochastic} - 1) \qquad \text{Equation 2}$$

where Ri is the ratio of i/44 CO_2 isotopologues, and Δ_{47} and Δ_{48} values are given in parts per thousand (‰).[2,9]

The precise measurement of Δ_{47} was enabled by modification of the Thermo MAT 253, specially configured with m/z 47-49 Faraday cups and digestion and purification methods for carbonate minerals.[2,8] Several studies have improved the accuracy and precision of Δ_{47} determinations by mass spectrometry. Interlaboratory reproducibility of sample Δ_{47} values was advanced by using accurately determined carbonate standard values that are anchored to the absolute reference frame, using a reference frame constructed using primary gas standards, secondary carbonate standards, or a mixture as anchors, detailed by Dennis et al.[10], allowing for interlaboratory standardization. Recent work from Bernasconi et al.[11] has proposed Δ_{47} carbonate standard anchor values and presented a proposal for Δ_{47} carbonate standardization in the 90 ^{o}C reference frame based on data from multiple labs, that has been further validated using long-term datasets[31].

Measurements of m/z 48 CO_2 for geothermometry and the study of kinetic effects have been explored recently, due to the use of 10^{13} Ω resistors for m/z 47-49 Faraday cups in the Thermo MAT 253 Plus[7,12–14], and the use of secondary electron suppression in the Nu Perspective IS (used here), which facilitates paired analysis of m/z 47 and m/z 48 CO_2 isotopologues for carbonate standards and unknown samples. The paired analysis of Δ_{47} and Δ_{48} measurements has been shown by theory[1,4,5,27,28] and experimentation[7,12–14] to have a characteristic equilibrium relationship to temperature which may be used to examine kinetic effects observed in biotic and abiotic samples, if these isotopic ratios can be accurately and precisely determined.

However, due to the low abundance of m/z 48 CO_2 isotopologues and potential for analytical error, the development of robust standard values and data quality assurance procedures is critical in ensuring accurate determination of unknown sample Δ_{48} values. Therefore, here we use both equilibrated gas and carbonate-based standardization to report Δ_{47} and Δ_{48} values for 27 carbonates, including 23 standards and 4 carbonates from Devils Hole[29,30], determined on different mass spectrometer configurations over multiple years. We use this data and theory to explore the equilibrium Δ_{47} and Δ_{48} relationship. We also report statistical methods for data processing and determine a regression-form acid digestion fractionation factor for the phosphoric acid digestion of m/z 63 and m/z 64 CO_3^{2-} to m/z 47 and m/z 48 CO_2, respectively.

1. EXPERIMENTAL DESIGN

1.1 Overview

Analyses for 27 carbonates (Table 1) are from 3 mass spectrometers using 5 instrumental configurations (Table 2), with varying acid digestion systems and temperatures, ion beam intensities, integration time, and standardization methods. Previous work using these sppecific mass spectrometer configurations by Upadhyay et al.[31] and Defliese and Tripati[32] established that Δ_{47} can be accurately determined with statistically indistinguishable values, and we sought to determine if this is possible for the coupled measurement of Δ_{47} and Δ_{48}. The data we present here consists of 1) $\Delta_{47\ \mathrm{CDES}\ 90}$ and $\Delta_{48\ \mathrm{CDES}\ 90}$ data determined using 25 °C and 1000 °C equilibrated gas-based standardization, 2) $\Delta_{47\ \mathrm{I\text{-}CDES}}$ (which is the same as $\Delta_{47\ \mathrm{CDES}\ 90}$ values if accurately anchored and determined) and $\Delta_{48\ \mathrm{CDES}\ 90}$ data determined using exclusively carbonate-based standardization.

We present an experimental regression between Δ_{47} and Δ_{48} values for 20 carbonates. Additionally, by comparing experimental data to calcite mineral theoretical equilibrium[4,5] we present a temperature-dependent equilibrium regression for 0-1000 °C. The Δ_{47}- Δ_{48} equilibrium regressions determined here are compared to equilibrium regressions from previous work[12–14]. We compare Devils Hole Δ_{48} and Δ_{47} values from this study to previous work[12,14,33]. We also develop regression-form acid digestion fractionation factors associated with the phosphoric acid digestion of calcite mineral into CO_2 gas, $\Delta^*_{63\text{-}47}$ and $\Delta^*_{64\text{-}48}$.

For this work, we also sought to develop robust statistical methods for quality control to further improve accuracy, precision, and interlaboratory reproducibility. We explicitly state how outliers and sample mean values were determined using this method and share R scripts for broader use.

1.2 Carbonates analyzed

In total, 27 different carbonates were analyzed for clumped and bulk isotope compositions. See Table 2 for a description of the mineralogy and origin of all carbonates, modified from Upadhyay et al.[31] These materials were chosen for analysis because many of them are standards used widely among clumped isotope laboratories, such as the ETH standards and Carrara Marble. Others are used commonly in a certain region or country, such as ISTB-1, TB-1, and TB-2, which are clumped isotope standards from the China University of Geosciences. Additionally, this suite of samples encompasses numerous carbonate types, including biogenic materials, and carbonates of different mineralogies. Some of the samples are presumed to have near equilibrium clumped isotope values, such as Devils Hole mammillary calcite, ETH-1, and ETH-2. Many also have a large number of analyses (n > 50) on one or multiple instruments that can be used to provide robust standard values for Δ_{47} and Δ_{48} measurements on the absolute reference frame.

2. METHODS

We determined coupled Δ_{47} and Δ_{48} values for 24 carbonates, and Δ_{47} values alone for 27 carbonates, on five mass spectrometer configurations in the Tripati Lab at the University of California, Los Angeles. The carbonates analyzed include the standards ETH-1, ETH-2, ETH-3, ETH-4, IAEA-1, IAEA-2, and Merck, which are used for interlaboratory comparisons. The Devils Hole mammillary calcite was also used for interlaboratory comparison.

In summary, we determined the $\Delta_{47\ \mathrm{CDES}\ 90}$ values of 7 carbonates using 25 °C and 1000 °C equilibrated gas-based standardization. This was done solely to compare Δ_{47} values produced in this study to other recently published work using equilibrated gas-based standardization. Our

$\Delta_{47\ CDES\ 90}$ values determined for ETH 1, ETH-2, ETH-3, and ETH-4 were in good agreement with the multi-laboratory determined $\Delta_{47\ CDES\ 90}$ values from Bernasconi et al.[11].

We used the $\Delta_{47\ CDES\ 90}$ values for ETH-1, ETH-2, and ETH-3 determined in Bernasconi et al.[11] in combination with two additional carbonate standards as anchors for carbonate-based standardization on four mass spectrometer configurations.

Similarly, $\Delta_{48\ CDES\ 90}$ values were determined for 7 carbonates, including ETH-1, ETH-2, and ETH-3, using equilibrated gas-based standardization. Because there are no agreed-upon Δ_{48} values for carbonate standards, the $\Delta_{48\ CDES\ 90}$ values determined here using equilibrated gas-based standardization were used as anchor values for carbonate-based standardization for unknown Δ_{48} data on three mass spectrometer configurations.

2.1 Equilibrated gas standards

We analyzed 195 equilibrated gas standards on a Nu Instruments Perspective mass spectrometer, here called Nu Perspective-EG. We utilized two gases with differing bulk isotope values, with a ~60 ‰ difference in δ_{47} values, prepared using standard procedures[2,10]9/17/2021 2:27:00 PM. The heavy isotope depleted δ_{47} gas is from an Airgas CO_2 gas cylinder and was equilibrated with 5-10 mL of 25 ^{o}C deionized (DI) water. The heavy isotope enriched δ_{47} gas is produced by phosphoric acid digestion of a Carrara Marble carbonate standard. The produced carbon dioxide was equilibrated with evaporated DI water held at 25 ^{o}C. Aliquots of the two 25 ^{o}C gases are re-equilibrated at 1000 ^{o}C by heating the gases in quartz tubes inside a muffle furnace for >1 hour, and then flash cooled, to produce gases with near stochastic Δ_{47} values.

2.2 Carbonate Standards

2.2.a. Carbonate standards used as anchors for data corrections

Anchor standards are used in corrections applied to all samples, as described in detail in Sections 2.5.a-2.5.d. Carbonate standards ETH-1 (n = 767), ETH-2 (n = 726), and ETH-3 (n = 463) were measured on Nu Perspective-1, Nu Perspective-1a, Nu Perspective-2, and MAT 253, and used as Δ_{47} anchors, as suggested by Bernasconi et al.[11] due to their different bulk isotope compositions, allowing for adequate linearity and scale compression corrections. These standards are widely available and have been routinely analyzed in our laboratory since 2014. Nu Perspective-2 used two additional anchors, Carmel Chalk (n = 640) and Veinstrom (n = 728), which are internal standards that have been routinely analyzed in our laboratory.

Anchor standards were also used for Δ_{48} data processing. The standards used as $\Delta_{48\ CDES\ 90}$ anchors for Nu Perspective-1, Nu Perspective-1a, and Nu Perspective-2 were ETH-1 (n = 464), ETH-2 (n = 439), and ETH-3 (n = 236). Nu Perspective-2 used one additional anchor standard, Veinstrom (n = 436).

2.2.b. Consistency standards

We used a suite of "consistency" standards, whose values were treated as unknowns, to ensure reproducibility across mass spectrometer configurations. The $\Delta_{47\ \mathrm{I\text{-}CDES}}$ consistency standards used for comparison between Nu Perspective-1, Nu Perspective-2, and MAT 253 were Carrara Marble and ETH-4. $\Delta_{47\ \mathrm{I\text{-}CDES}}$ consistency standards used for comparison between Nu Perspective-2 and MAT 253 were CM Tile, IAEA-C1, IAEA-C2, and Merck. $\Delta_{47\ \mathrm{I\text{-}CDES}}$ consistency standards used for comparison between Nu Perspective-1 and MAT 253 were Carmel Chalk and TV03.

The $\Delta_{48\ \mathrm{CDES}\ 90}$ consistency standards used for comparison between Nu Perspective-1 and Nu Perspective-2 were Carmel Chalk, Carrara Marble, CM Tile, and ETH-4.

2.2.c. Additional samples

These samples were analyzed either on only one mass spectrometer configuration or their value was averaged from more than one configuration because of n < 9 (see Section 3.2) replicates per configuration. The additional samples include SRM 88B, 102-GC-AZ01, 47407 Coral, ISTB-1, Mallinckrodt, NBS-19, Spel 2-8-E, TB-1, TB-2, and TV01.

2.3 Devils Hole calcite

Four samples of mammillary calcite from Devils Hole (DH) core DH-2[29], Amargosa Desert, Nevada were analyzed for $\Delta_{47\ \mathrm{I\text{-}CDES}}$ and $\Delta_{48\ \mathrm{CDES}\ 90}$ values. Devils Hole calcite is assumed to have precipitated near isotopic equilibrium due to an extremely slow precipitation rate (0.1-0.8 µm year^{-1}), low calcite saturation index (0.16-0.21) and a stable temperature of 33.7 (±0.8) ^{o}C throughout the Holocene.[29,30,34,35] DH samples were analyzed for use in the construction of a Δ_{47} and Δ_{48} equilibrium relationship, and in the determination of the acid digestion fractionation factors from calcite mineral to CO_2 gas, $\Delta^*_{63\text{-}47}$ and $\Delta^*_{64\text{-}48}$. The DH samples reported here are from sections 10 (172 ± 4 ka), 11 (163 ± 4 ka), 12 (157 ± 5 ka), and 13 (151 ± 5 ka).[29]

2.4 Instrumentation

Standards and unknowns were analyzed on 3 mass spectrometers using 5 configurations (Table 2). Nu Perspective-EG, Nu Perspective-1, and Nu Perspective-1a use the same mass spectrometer with differences in the acid digestion system, ion beam intensity, integration time, and mode of standardization. Nu Perspective-EG is the only configuration that analyzed equilibrated gases. All Nu Perspective configurations utilized sample masses of 0.45-0.60 mg. On both the MAT 253 and Nu Perspective mass spectrometers, the detectors for *m/z* 44 through 46 are registered through 3×10^8, 3×10^{10}, and 10^{11} Ω resistors, respectively, while detectors for *m/z* 47 through 49 are registered with 10^{12} Ω resistors. One of the most notable differences between the Nu Instruments Perspective IS and the more widely used Thermo Fisher MAT 253 is the use of secondary electron suppression achieved by two curved plates with a voltage difference placed in front of the Faraday collectors for *m/z* 47-49. This advancement has contributed to a Δ_{47} non-linearity slope for the Nu Perspective (median slope observed was -0.00005) that ranges from one to two orders of magnitude less than the MAT 253 (median slope observed was -0.007), and a Δ_{48} non-linearity slope for the Nu Perspective (median slope observed was -0.004) that is an order of magnitude less than the MAT 253 (median slope observed was -0.013). The resulting improvements in accuracy and precision enabled the Nu Perspective mass spectrometers to yield reproducible Δ_{48} data, while the Δ_{48} data produced on the older generation MAT 253 may only be applicable in some situations (see Results).

The Nu Perspective-EG, Nu Perspective-1, Nu Perspective-1a, and MAT 253 use an in-house constructed autosampler that is similar to the setup detailed in Passey et al.[36] The configuration uses a stainless steel Costech Zero Blank autosampler, a 105 % phosphoric acid bath that digests calcium carbonate samples at 90 ^{o}C. The sample gas passes through cryogenic purification traps that use dry ice-cooled ethanol and liquid nitrogen to remove contaminant gases that have low vapor pressure, mostly consisting of water vapor. The CO_2 gas then passes through elemental silver wool (Sigma-Aldrich) to remove sulfur compounds, followed by a gas chromatograph (GC) column with helium carrier gas that contains Porapak Type-Q^{TM} 50/80 mesh column packing material to remove organic compounds. The GC column is maintained at a constant temperature of -20 ^{o}C during sample purification. Large samples (4-7 mg) are analyzed on the MAT 253 in bellows with a total integration time of 720 s. Small samples (0.5 mg) are analyzed in microvolume mode on the Nu Perspective with 3 blocks of 20 cycles, with a total integration time of 1600 s. The sample and working gas volumes are depleted in microvolume mode at precisely matched rates, with *m/z* 44 ranging from 80-30 nA during sample acquisition. The sample preparation system is operated by custom software in Labview that controls the sampler, GC column, cryogenic dewar lifters, and valves. The Labview software is integrated with the Perspective Stable Gas Control software interface that controls the Nu Perspective mass spectrometer.

Nu Perspective-2 uses a Nu Carb Sample Digestion System instead of a common acid bath, where calcium carbonate is reacted at 70 ^{o}C in individual glass vials with 105 wt% phosphoric acid. This eliminates the use of a common acid bath. The sample gas is cryogenically purified in liquid nitrogen-cooled tubes called coldfingers before passing into a relatively short GC column packed with Porapak Type-Q^{TM} 50/80 and silver wool. This instrument operates under vacuum pressure and does not use a carrier gas. The sample and working gas volumes are matched precisely during depletion into the mass spectrometer. Sample data is analyzed in three blocks of 20 cycles, with each cycle integrating for 20 s, for a total integration time of 1200 s.

2.5 Corrections applied to Δ_{47} and Δ_{48}

Raw data files (Isodat results files from the MAT 253, data text files from the Nu instruments) from all instrument configurations were transferred into Easotope[37] (64-bit version from release 20201231), where corrections and final Δ_{47} and Δ_{48} values for individual replicates and standards were calculated. All data used the IUPAC parameter set.[38,39] Average values for each sample were calculated, and the external error is reported as 1 standard error (SE) considering all replicates included in the final data pool[40]. Because most of the samples reported have multiple replicates analyzed over multiple years, this represents the long-term SE, which is typically higher than SE associated with a small number of replicates analyzed in a single standardization window or short time interval. We note this may not fully account for all error associated with transferring raw data into the final Δ_{47} values, described as "allogenic" errors by Daëron (2021). The same is true for Δ_{48}.

2.5.a Equilibrated gas-based nonlinearity corrections

The Nu Perspective-EG was the only configuration in this study that used equilibrated gases to determine nonlinearity slope corrections. A combined slope was determined over a 10-day moving average for the regression lines between $\delta_{47\ \mathrm{raw}}$ and $\Delta_{47\ \mathrm{raw}}$, and $\delta_{48\ \mathrm{raw}}$ values relative to $\Delta_{48\ \mathrm{raw}}$ values for CO_2 gas standards equilibrated at 25 ^{o}C and 1000 ^{o}C (Figure 1a- b). Nonlinearity slope corrections are applied to all samples using Equations 3 and 4

$$\Delta_{47\ \mathrm{sc}} = \Delta_{47\ \mathrm{raw}} - (m_{47} \times \delta_{47\ \mathrm{raw}}) \qquad \text{(Equation 3)}$$

$$\Delta_{48\ \mathrm{sc}} = \Delta_{48\ \mathrm{raw}} - (m_{48} \times \delta_{48\ \mathrm{raw}}) \qquad \text{(Equation 4)}$$

where $\Delta_{47\ \mathrm{sc}}$ and $\Delta_{48\ \mathrm{sc}}$ values (Figure 2) are the nonlinearity slope-corrected $\Delta_{47\ \mathrm{raw}}$ and $\Delta_{48\ \mathrm{raw}}$, and m_{47} and m_{48} are the regression slopes, with nomenclature adapted from Fiebig et al.[7] The gas-based slope corrections for Nu Perspective-EG can be found in Supplementary Tables S1 and S2.

2.5.b Carbonate standard-based non-linearity corrections

For Nu Perspective-1, and Nu Perspective-1a, Nu Perspective-2, and MAT 253, ETH-1 and ETH-2 were used to determine 10-day moving average nonlinearity slopes for the regression lines between $\delta_{47\ \mathrm{raw}}$ and $\Delta_{47\ \mathrm{raw}}$, and $\delta_{48\ \mathrm{raw}}$ relative to $\Delta_{48\ \mathrm{raw}}$ values (Figure 1c-h). The slopes were then used in Equations 3 and 4 to determine the nonlinearity slope corrections for all samples (Figure 2). The carbonate-based slope corrections for Nu Perspective-1, Nu Perspective-1a, Nu Perspective-2, and MAT 253 can be found in Supplementary Tables S3-S14.

2.5.c Δ_{47} and Δ_{48} values determined using equilibrated gas-based standardization

The Nu Perspective-EG was the only configuration used in this study that used equilibrated gas-based standardization. $\Delta_{47\ sc}$ and $\Delta_{48\ sc}$ values were projected into the Carbon Dioxide Equilibrium Scale in the 90 ^{o}C absolute reference frame (CDES 90), using methods detailed in Dennis et al.[10] and nomenclature adapted from Fiebig et al.[7] The 10-day moving average slope and intercept was determined for the linear relationship between theoretically calculated Δ_{47} values for 25 ^{o}C and 1000 ^{o}C, 0.925 ‰[41] and 0.027 ‰[10], respectively, and $\Delta_{47\ sc}$ values. This was also done for theoretically calculated Δ_{48} values for 25 ^{o}C and 1000 ^{o}C of 0.345 ‰[41] and 0.000 ‰[7], respectively, and $\Delta_{48\ sc}$. The equilibrated gas transfer function (EGTF) slope and intercept from these regressions (Figure 3a-b) were used to create empirical transfer functions, which are applied to all $\Delta_{47\ sc}$ and $\Delta_{48\ sc}$ values on Nu Perspective-EG, and yields the fully corrected values $\Delta_{47\ CDES\ 90}$ and $\Delta_{48\ CDES\ 90}$ values (Figure 2), using Equations 5 and 6

$$\Delta_{47\ CDES\ 90} = \Delta_{47\ sc} \times \text{EGTF slope} + \text{EGTF intercept} \qquad \text{Equation 5}$$

$$\Delta_{48\ CDES\ 90} = \Delta_{48\ sc} \times \text{EGTF slope} + \text{EGTF intercept} \qquad \text{Equation 6}$$

where $\Delta_{47\ CDES\ 90}$ and $\Delta_{48\ CDES\ 90}$ values are the fully corrected values digested in phosphoric acid at 90 ^{o}C, $\Delta_{47\ sc}$ and $\Delta_{48\ sc}$ values are the slope corrected values from Equations 3 and 4, EGTF slope is the equilibrated gas transfer function slope, and EGTF intercept is the equilibrated gas transfer function intercept. We have chosen to omit the acid fractionation factor (AFF) correction that was historically used to transfer fully corrected 90 ^{o}C values into the 25 ^{o}C reference frame, $\Delta^{*}_{47\ 90\text{-}25}$, to avoid the additional error potentially associated with this transformation, given that $\Delta^{*}_{47\ 90\text{-}25}$ is poorly constrained and there is currently no known $\Delta^{*}_{48\ 90\text{-}25}$. All equilibrated gas-based transfer function slopes and intercepts are in Supplementary Tables S1 and S2.

2.5.d Δ_{47} values in the I-CDES reference frame

The Nu Perspective-1, Nu Perspective-1a, Nu Perspective-2, and MAT 253 used carbonate-based standardization. We present our data in the Intercarb-Carbon Dioxide Equilibrium Scale (I-CDES) reference frame, $\Delta_{47\ I\text{-}CDES}$, which was developed after comparing the data from 25 mass spectrometers in 22 laboratories to determine nominal carbonate standard values for ETH-1, ETH-2, and ETH-3 for use in applying data corrections in a consistent way, thereby increasing reproducibility.[11] I-CDES is in the 90 ^{o}C reference frame, which omits the practice of transferring final data into the 25 ^{o}C reference frame and the associated error, given that many measurements are done with acid digestion temperatures of 70-100 ^{o}C. This approach potentially increases interlaboratory reproducibility by using well-constrained $\Delta_{47\ I\text{-}CDES}$ values for widely available carbonate standards (ETH-1, ETH-2, ETH-3) as “anchors” for corrections. The $\Delta_{47\ I\text{-}CDES}$ values determined in Bernasconi et al.[11] of 0.2052 ‰, 0.2085 ‰, and 0.6132 ‰ were used as anchor values for ETH-1, ETH-2, and ETH-3, respectively, for transfer functions.

However, the calculations used here differ from the procedure used in Bernasconi et al[11]. In Bernasconi et al.[11], a single equation is used to account for nonlinearity slope corrections and transferring raw Δ_{47} values into the absolute reference frame. Here, we use separate equations for nonlinearity slope corrections (Equation 3) and to transfer data into the absolute reference frame (Equation 7). Because our linearity corrections are constructed using ETH-1 and ETH-2, and our transfer functions are constructed with ETH-1, ETH-2, and ETH-3 using I-CDES values, we are confident that our final Δ_{47} values are adequately transformed into the I-CDES reference frame; Daëron[42] described the approaches used here and in Bernasconi et al.[11] as mathematically equivalent.

The 10-day moving average slope and intercept was determined for the linear relationship between the ETH-1, ETH-2, and ETH-3 $\Delta_{47\ \text{I-CDES}}$ anchor values and the $\Delta_{47\ \text{SC}}$ values (Figure 3c). To create our carbonate standard based transfer functions (CSTF) applied to standards and unknown samples, the slope and intercept from these regressions are used in Equation 7

$$\Delta_{47\ \text{I-CDES}} = \Delta_{47\ \text{sc}} \times \text{CSTF slope} + \text{CSTF intercept} \qquad \text{Equation 7}$$

where $\Delta_{47\ \text{I-CDES}}$ is the fully corrected value in the I-CDES reference frame at 90 ^{o}C (Figure 2a), $\Delta_{47\ \text{sc}}$ is the slope corrected value from Equation 3, CSTF slope is the carbonate standard transfer function slope, and CSTF intercept is the carbonate standard transfer function intercept. All carbonate-based Δ_{47} transfer function slopes and intercept are available in Supplementary Tables S3, S5, S7, S9, S11, and S13.

Nu Perspective-2 uses the same method detailed above with the additional standards Carmel Chalk and Veinstrom used as anchors for transfer functions. The anchor $\Delta_{47\ \text{I-CDES}}$ values used for Carmel Chalk and Veinstrom were 0.674 ‰ and 0.715 ‰, respectively. Before Carmel Chalk and Veinstrom were used as anchors in Nu Perspective-2, their long-term average values were determined in the I-CDES reference frame on Nu Perspective-1 and MAT 253 using the method described above. Additionally, Nu Perspective-2 is the only mass spectrometer used here with a 70 ^{o}C acid digestion temperature, with the other instruments having an acid digestion temperature of 90 ^{o}C. Equation 7 is used to stretch data produced on Nu Perspective-2 into the 90 ^{o}C reference frame, therefore, no additional acid fractionation factor is applied.

2.5.e Δ_{48} using carbonate standard-based corrections

For carbonate-based standardization on Nu Perspective-1, Nu Perspective-1a, Nu Perspective-2, mean $\Delta_{48\ \text{CDES 90}}$ standard values determined on Nu Perspective-EG using 25 ^{o}C and 1000 ^{o}C equilibrated gas corrections were used as anchor values. Nu Perspective-1, Nu Perspective-1a, and Nu Perspective-2 used ETH-1, ETH-2, and ETH-3 as anchors. Nu Perspective-2 used Veinstrom as an additional anchor, and MAT 253 used Carrara Marble and Veinstrom as additional anchors. The 10-day moving average slope and intercept were determined for the linear relationship between the $\Delta_{48\ \text{CDES 90}}$ anchor values and the $\Delta_{48\ \text{sc}}$ values

(Figure 3d). To create carbonate standard transfer functions (CSTF) that are applied to all standards and unknown samples, the slope and intercept from these regressions are used in equation 8,

$$\Delta_{48\ \mathrm{CDES}} = \Delta_{48\ \mathrm{sc}} \times \text{CSTF slope} + \text{CSTF intercept} \qquad \text{Equation 8}$$

where $\Delta_{48\ \mathrm{CDES\ 90}}$ is the fully corrected value in the CDES 90 reference frame (Figure 2b), $\Delta_{48\ \mathrm{sc}}$ is the slope-corrected value from Equation 4, CSTF slope is the carbonate standard transfer function slope, and CSTF intercept is the carbonate standard transfer function intercept. All carbonate-based Δ_{48} transfer function slopes and intercepts are available in Supplementary Tables S4, S6, S8, S10, S12, and S14.

Δ_{48} data from the MAT 23 was standardized using ETH-1, ETH-2, ETH-3, Carrara Marble, and Veinstrom as anchors. $\Delta_{48\ \mathrm{CDES\ 90}}$ data from the MAT 253 was examined for exploratory purposes and was not pooled with Nu Perspective data.

2.6 Use of statistical methods for robust determination of Δ_{47} and Δ_{48} values

Several studies have used different criteria for replicate-level outlier identification and data pooling for different instruments. For outlier identification, one group of publications use outlier tests. Zaarur et al.[43] used a Pierce outlier test to identify and remove replicate Δ_{47}, □^{18}O, and □^{13}C values that are statistical outliers, resulting in the exclusion of ~2% of data. They report this affected Δ_{47} in the third decimal place. Burgener et al.[44] used this same test to determine one sample Δ_{47} value was an outlier relative to the other samples in the dataset. Peral et al.[45] used Grubbs' outlier test to show that a Δ_{47} value for a foraminifera sample was an outlier when compared to the rest of their sample set. Caution with each of the above specific outlier-based tests is warranted, as the concept of an outlier is not meaningful in the absence of a normal distribution. A second group of publications have used absolute deviations from mean values as cutoffs. Meckler et al.[46] excluded standard replicates with an offset greater than ± 0.03 ‰ from the mean value in each run. Upadhyay et al.[31] excluded replicates with an offset greater than ± 0.075 ‰ from the mean value. A third group of publications uses ancillary data. Tripati et al.[5] use Δ_{48} values of > 1 per mil (Δ_{48} excess) to be potentially indicative of contamination, and screened data if replicate level □^{13}C or □^{18}O values differed from the population mean by more than 3σ. Tripati et al.[17] used Δ_{48} excess, and also used a Q-test (which identifies outliers at a 5σ level), for data quality assurance. Bernasconi et al.[11] worked with data that was provided by labs, based on each lab's own criteria for quality assurance to produce publication-grade results.

For data pooling from multiple instruments, Bernasconi et al.[11] received pressure-baseline corrected data for carbonate standards from 22 laboratories and used a single Python script to perform standardization, data corrections, and error propagation. Their final pooled Δ_{47} values were error weighted. Bonifacie et al.[47] analyzed 12 dolomite samples with precipitation temperatures between 25 °C to 351 °C at two separate laboratories, with each laboratory using different instrumentation and standardization methods. They described sample average Δ_{47} values from each laboratory as indistinguishable and determined pooled sample average values. They also combined their data with previously published data from 7 laboratories to determine a Δ_{47}-T calibration for use in (Ca, Mg, Fe)CO_3. They did this by using only data in the CDES[10] reference frame, averaging data by formation temperature, and weighting data by error and number of replicates for carbonate standards from each study.

Below, we provide a detailed description of a proposed method for replicate-level outlier identification and data pooling from multiple instruments that yield statistically indistinguishable Δ_{47} and Δ_{48} values. The statistical analyses described below were performed in R version 4.0.4[48]. R code and raw data used in analyses are publicly available for review at https://github.com/Tripati-Lab/Lucarelli-et-al. Following acceptance for publication, code and raw data will be permanently archived on Dryad, and this section will be updated with a static link.

2.6.a Statistical techniques used for data quality assurance

For Δ_{47} and Δ_{48} quality assurance, we adapted screening criteria used in other disciplines, implementing kernel density estimation as a statistical technique for use with clumped isotope data. Kernel density estimation has a broad range of research applications, including economics[49], ecology[50], climate modeling[51], weather forecasting[52], and manufacturing controls[53], among others. The data processing steps are outlined in Figure 4, and a comprehensive guide to using the technique is provided in Supporting Information Appendix A. In brief, for each standard reported here, we completed quality assurance of raw data by screening replicates using kernel density estimation to identify and eliminate extreme (i.e., inaccurate) or poorly constrained (imprecise with high internal error) values that would either be hand-selected for removal or identified with an outlier test. The kernel density estimate may be described as a smoothed histogram, with the benefit that calculation of the smooth does not depend on knowing beforehand the distribution of the data.

We evaluated the impact of using a 3σ or 5σ cutoff on sample mean values and uncertainties (Figures 5c-f; 6-7; Table 4). When considering Δ_{47} values for the anchor standards ETH-1 and ETH-2 on Nu-Perspective-1 (Figure 6 a, b), Nu-Perspective-2 (Figure 6 e, f), and MAT 253 (Figure 6 i, j), we find that the average absolute difference in final mean between 3σ and 5σ cutoffs is 0.0005 ‰ (median 0.0003 ‰, max 0.0017 ‰); absolute difference in standard deviation is 0.001 ‰ (median 0.0004 ‰, max 0.0034 ‰); and number of replicates excluded on average increases by 1.7 (median 1, max 4) with the more stringent 3σ cutoff. For the consistency standards ETH-4 (Figure 6 c, g, k) and Veinstrom (Figure 6 d, h, l), the average absolute difference in final mean is 0.0003 ‰ (median 0.0003 ‰, max 0.0009); average absolute difference in standard deviation is 0.0005 ‰ (median 0.0004 ‰, max 0.0015 ‰); and the number of replicates excluded on average increases by 0.83 (median 1, max 2) with the more stringent cutoff. Comparing Δ_{48} values for the anchor standards ETH-1 and ETH-2 on Nu-

Perspective-1 (Figure 7 a, b) and Nu-Perspective-2 (Figure 7 e, f) using a 3σ or 5σ cutoff, we find that the average absolute difference in final means is 0.0001 ‰ (median 0 ‰, max 0.0005 ‰); average absolute difference in standard deviation is 0.0006 ‰ (median 0.0004 ‰, max 0.0018 ‰); and the number of replicates excluded on average increases by 0.75 (median 0.5, max 2) with the more stringent cutoff. For the non-anchor standards ETH-4 (Figure 7 c, g) and Veinstrom Figure 7 d, h), we find no difference in the final datasets between 3σ and 5σ cutoffs for either Nu-Perspective-1 or Nu-Perspective-2. This comparison, and unpublished comparisons we have done, show that 3σ and 5σ cutoffs yield comparable results.

Thus, we use a 3σ cutoff, which was sufficient to capture the entire distribution peak for all samples. The remaining replicates were then tested for normality. The full quality assurance process led to the elimination of an average of 5.0 % of replicates (median 3.3 %) for Δ_{47}, and an average of 6.4 % (median 4.4 %) for the more sensitive Δ_{48} analyses. We report the number of replicates excluded during the quality assurance process for each standard in Supplementary Tables S21 and S22.

The quality assurance process is described more fully here. For each standard of interest, we calculated a kernel density estimate using the generic S3 method ‘density’ included in base R’s stats package.[48] In quality screening of clumped isotope data, a nonparametric approach, such as kernel density estimation, is preferred because we often have no *a priori* knowledge of the statistical properties of the raw clumped isotope replicate pool. In density estimation, a weighting function, known as a kernel, is applied to the data; in the R implementation of kernel density estimation, the default is to use a normally distributed (Gaussian) kernel, K, applied to a variable, u. The normal distribution takes the form:

$$K(u) = \frac{1}{\sqrt{2\pi}} e^{-\frac{1}{2}u^2}$$

The smoothing parameter, known as bandwidth, using the default normally distributed kernel, is set to equal the standard deviation of the kernel, or weighting function, itself.[48] The kernel then becomes a curve that integrates to 1 with the statistical properties:

$$\sigma^2(K) = t^2 K(t)\, dt$$

For a full explanation of bandwidth selection in nonparametric probability density estimation, see Sheather & Jones[54]; for a full explanation of kernel density estimation as implemented in R, see Deng & Wickham[55].

Kernel density estimation is used to examine the underlying probability density function (PDF) for a given variable. Each measured clumped isotope value is not a single definite point, due to the uncertainty inherent in measurement, but is rather a finite probable range of values. This can be visualized as a peak where the most probable values for a given variable cluster together to produce the peak’s maxima; this is the probability density function. This is similar to the way in which histograms demonstrate data distributions based on counts (Figure 5a). From the PDF peak for each standard, we found the nearest minima, or least probable values of the possible range, on either side of the maxima, or most probable value, and defined those minima as the initial cutpoints for exclusion (Figure 5b). In cases where the PDF revealed a double peak or a shoulder at least a third as high as the true maxima, we used the second nearest minima or left/right minima according to the shape of the density peak. These cases are fully described in Supporting Information Appendix A, along with a user guide to the quality control and data screening process. The density-based minima exclusion method has been included as a custom function in the accompanying R script, Supporting Information Appendix B (available on GitHub; all code and data will be permanently archived on Dryad upon acceptance for publication and a static link make available here), and instructions for its use are given in the script. Hereafter, we refer to this statistical technique as the "nearest minima method" for the sake of brevity.

Following initial screening based on the nearest minima, we employed a 3σ exclusion which yielded results for Δ_{48} that were consistent across instruments (Figure 5c). A Shapiro-Wilk test was used to determine whether the resulting data were consistent with a normal distribution. A visual representation of the data at each step in this process is included in Figure 5, with the final replicate pool shown as a histogram in Figure 5d.

2.6.b Inter-instrumental comparisons and data pooling

Five mass spectrometer configurations, as described in section 2.4 and Table 2, were used to measure clumped isotopes in this study. Previous work has shown that carbonate-based standardization, as performed here, can produce statistically indistinguishable results from different mass spectrometer systems, including Nu Perspective and MAT 253[11,56]. Despite differences in the mass spectrometer configurations used in this study, the long-term external reproducibility for Δ_{47} and Δ_{48} is similar for all configurations (Table 2), likely due to the high frequency and large number of standards analyzed on each instrument, and the use of identical data processing methods. Due to the similar long-term instrumental reproducibility and high replicate number for most carbonates analyzed, we have not weighted our final Δ_{47} and Δ_{48} values.

Quality assurance for replicate data from each configuration was conducted using the nearest minima method described in section 2.6.a. To test for any differences between configurations that would preclude pooling data for analyses, we modeled final clumped isotope values by the additive effects of configuration and standard using a linear mixed effects model from package *nlme* version 3.1-152[57] after Upadhyay et al.[31] Linear mixed effects models provide a convenient extension to conventional linear models, in that they allow for both fixed effects (the independent variables) and random effects (additional variables which may affect the dependent variables, but which are not being explicitly modeled). The standard error of the final clumped isotope value was included as a random effect in the model. Models did not include carbonates that were run rarely on these instruments, and for which we have few replicates (ISTB-1, TB-1, TB-2, CIT Carrara, DH-2-10, DH-2-11, DH-2-12, DH-2-13, TV01, 47407 Coral, Spel-2-8-E, and 102-GC-AZ01).

To ensure it was appropriate to pool data produced using different mass spectrometer configurations, we performed statistical tests comparing individual sample mean values produced on each configuration and also the overall cumulative comparability of each configuration. Pairwise differences between configurations were then assessed using contrasts with adjustment for multiple comparisons from package *emmeans* version 1.5.4.[58] Estimated marginal means are preferred to ordinary marginal means because they control for differences in the number of analyses run on individual configurations, *i.e.*, a configuration running more standards overall, or more replicates of a particular standard, is not given more weight in the pairwise analysis than one running fewer. Data were pooled for further analyses only if there was no evidence of a statistically significant difference between configurations across any of the samples reported herein. We also did not pool together data calculated using gas-based standardization and carbonate-based standardization.

2.6.c Power analysis to estimate the number of replicates needed

We employed power analysis to determine the number of replicates needed to reach the overall mean for each sample's Δ_{47} and Δ_{48} values on each of the configurations. This was accomplished via the two-sample t-test power function in package pwr version 1.3-0.[40] Power is defined as the probability of correctly detecting an effect. The four key elements of statistical power are sample size, variation in the data, the error rate, and effect size. Power analysis back-calculates a minimum required sample size given the other three elements. We used a power, or probability of detection, of 95 % and an α, or probability of false positive error, of 0.05 (5 %). Cohen's d, the effect size, is widely used to compare differences between two means. Cohen's d in the power analysis was populated with the overall mean and standard deviation of the final, quality-controlled replicate pool for each sample. The power analysis then returned an estimate, for each sample, of the number of replicates required for the mean of their values to become statistically indistinguishable from the overall mean of all replicates included in this study. The number of required replicates for each sample was averaged to produce recommendations for replication on each configuration. We excluded samples for which the recommended number of replicates was greater than the number of replicates included in our dataset. Sample replicate recommendations should be interpreted as the typical minimum number of replicates needed after the exclusion of poorly constrained replicates via the nearest minima method described in section 2.6.a.

3. RESULTS AND DISCUSSION

3.1 Instrumental configuration comparison

We found no evidence of statistically significant differences in final clumped isotope values between configurations for either $\Delta_{47\ \text{I-CDES}}$ or $\Delta_{48\ \text{CDES 90}}$ (Table 3, SI Figures S1, S2). In general, we find that different instrument configurations can produce comparable values. However, Δ_{48} data from the MAT 253 were not pooled with Nu Perspective-1 and Nu Perspective-2 results because offsets were observed in anchor standards ETH-1 and ETH-2 (known equilibration temperature of 600 ^{o}C) that did not exist in Nu Perspective-1 and Nu Perspective-2 (Figure 8, SI Figure S4, Table 6). The older generation MAT 253 does not use secondary electron suppression, and therefore, does not yield as precise Δ_{48} data as the Nu Perspective instruments, which do use secondary electron suppression (see section 2.4). Nu Perspective-EG used gas-based standardization while Nu Perspective-1 and Nu Perspective-2 used carbonate-based standardization. We therefore present Δ_{47} and Δ_{48} analyses for Nu Perspective-EG individually, while Nu Perspective-1 and Nu Perspective-2 analyses were pooled.

3.2 Estimate of replicates needed by mass spectrometer configuration

Power analysis was used to determine the number of replicates necessary to achieve the overall mean for a given sample. These estimates are used to provide insight into the number of replicates that should typically be targeted for various configurations. Replicate recommendations are to be understood as the final pool of replicates per sample after elimination of replicates identified as poorly constrained via the nearest minima method. Factors that influence the number of required replicates include integration time and ion beam intensity, which vary between configurations (Table 2). Additional time- and condition-dependent factors that can influence reproducibility include signal/noise, instrument stability, linearity corrections, and cleanliness of measured gases. This analysis illustrates what is typical given long-term variability, and not necessarily what is characteristic of any given set of correction intervals for a particular instrument.

For Δ_{47} analyses we found that typically ~14 replicates per sample were needed for the Nu Perspective-1and MAT 253 to yield results that were statistically indistinguishable from the long-term mean. Approximately 3 replicates per sample were needed on Nu Perspective-2. We were not able to reliably determine the number of replicates needed for Nu Perspective-EG due to an insufficient number of replicates per sample required to successfully complete a power analysis.

For Δ_{48} analyses on Nu Perspective-EG, which is standardized with equilibrated gases only, we found that typically ~18 replicates were needed per sample. Nu Perspective-1 and Nu Perspective-2, which use carbonate standard-based standardization, typically required ~9 replicates per sample to yield results that were statistically indistinguishable from the long-term mean. MAT 253, which is an older generation mass spectrometer using carbonate-based standardization, typically required ~37 replicates.

3.3 Δ_{47} and Δ_{48} results determined using equilibrated gas-based standardization

$\Delta_{47\ \mathrm{CDES}\ 90}$ values were determined for 7 standards using 25 ^{o}C and 1000 ^{o}C equilibrated gas-based standardization, with a total of 324 analyses performed from May 2015-August 2016 on Nu Instruments-EG (Table 4). The long-term average $\Delta_{47\ \mathrm{CDES}\ 90}$ values for ETH-1, ETH-2, and ETH-3 determined here were within 1 SE of the nominal anchor values determined in Bernasconi et al.[11] (Figure 9a). The range of Δ_{47} offsets between the datasets for these three standards was 0.000 ‰ to 0.008 ‰. For ETH-4, the $\Delta_{47\ \mathrm{CDES}\ 90}$ offset observed between the two datasets is 0.012 ‰, which is <1 SD.

$\Delta_{48\ \mathrm{CDES}\ 90}$ values were determined for 7 standards using equilibrated gas-based standardization, with a total of 363 analyses performed from May 2015-June 2017. We have compared our $\Delta_{47\ \mathrm{CDES}\ 90}$ and $\Delta_{48\ \mathrm{CDES}\ 90}$ to other recently published datasets with paired clumped isotope values for ETH standards, Fiebig et al.[7], Bajnai et al.[12], and Swart et al.[13] (Figure 10, Table 5). The Δ_{47} error reported in all studies was similar (0.001 ‰ to 0.006 ‰); the range of Δ_{47} offsets between the datasets was 0.002 ‰ to 0.012 ‰, and 0.009 ‰ to 0.038 ‰ for Δ_{48} values. The Δ_{48} error reported in Bajnai et al.[12] of 0.004 ‰ to 0.005 ‰ was lower than that for the other studies which have error ranging from 0.007 ‰ to 0.014 ‰, possibly from more replication, larger sample size, and longer mass spectrometric integration times than what was used here.

3.4 Δ_{47} determined using carbonate-based standardization

$\Delta_{47\ \mathrm{I\text{-}CDES}}$ values were determined for 24 carbonates (27 including anchor standards) using ETH carbonate standard-based standardization, with a total of 5,211 analyses performed from April 2015-March 2021 on Nu Perspective 1, Nu Perspective 1a, Nu Perspective 2, and MAT 253 (Table 5). We used IAEA-C1, IAEA-C2, Merck, and ETH-4 as consistency standards for direct comparability across instrument configurations and to Bernasconi et al.[11] (Figure 9b). All instrument configurations produced $\Delta_{47\ \mathrm{I\text{-}CDES}}$ data that were statistically indistinguishable (Table 3) using a linear effects model described in detail in Section 2.6.b. All sample replicate data were normally distributed, with the exception of ETH-3 analyzed on MAT 253 (Supplementary Table S20). Data from different instrument configurations were pooled to determine a combined instrument long-term average (Table 6). The long-term combined instrument average for IAEA-C1, IAEA-C2, and Merck were within 1 SE, and ETH-4 was within <1 SD of values determined in Bernasconi et al.[11], which were determined with the combined data from 22 laboratories, including data from UCLA for a subset of correction intervals. Results are also consistent with the analysis of Upadhyay et al.[31]

3.5 Δ_{48} determined using carbonate-based standardization

$\Delta_{48\ \mathrm{CDES}\ 90}$ values were determined for 24 carbonates using ETH carbonate standard-based standardization, with a total of 3,037 analyses performed from April 2015-August 2020 on Nu Perspective-1, Nu Perspective-1a, and Nu Perspective-2 (Table 6). The $\Delta_{48\ \mathrm{CDES}\ 90}$ from these three instrument configurations were determined to be statistically indistinguishable (Table 3) and were pooled to determine a combined instrument average. All Δ_{48} replicate data were normally distributed (Supplementary Table S19).

We also present Δ_{48} data produced on the older generation MAT 253 mass spectrometer (Table 6). Due to higher error, lower precision, and offsets in ETH-1 and ETH-2 values, we did not pool Δ_{48} produced on the MAT 253 with the data produced on the Nu Perspective instruments. However, Δ_{48} data from the MAT 253 is included here due to the large amount of clumped isotope data produced on this instrument going back to 2014, considering comments from J. Eiler (pers. comm.) that these instruments may produce usable Δ_{48} data. We were curious as to whether this instrument, with sufficient replication and quality control, could produce usable Δ_{48} values. We observed that the MAT 253 produced similar average values for the majority of carbonates studied here (Table 6; SI Figure S4), with larger SE than the Nu Perspective instruments, as expected. All Δ_{48} replicate data produced on the MAT 253 were normally distributed except for ETH-1 (Supplementary Table 19). Thus, it may be worth mining past MAT 253 data depending on the reproducibility of measurements, although newer generation instrumentation is preferable for the measurement of Δ_{48} values for new samples.

3.6 Experimentally determined regression between Δ_{47} and Δ_{48}

The second-degree polynomial described by Equation 9 ($r^2 = 0.97$) was fit through 20 experimentally determined $\Delta_{47\ \mathrm{I\text{-}CDES}}$ and $\Delta_{48\ \mathrm{CDES}\ 90}$ values for carbonates, including standards and Devils Hole calcite, determined in this study (Figure 11).

Equation 9

$$\Delta_{48\ \mathrm{CDES}\ 90\ \mathrm{EQ}} = (0.1179 \pm 0.0266) - (0.0398 \pm 0.1332)\Delta_{47\ \mathrm{I\text{-}CDES\ EQ}} + (0.4407 \pm 0.1490)\Delta_{47\ \mathrm{I\text{-}CDES\ EQ}}^{2}$$

All $\Delta_{48\ \mathrm{I\text{-}CDES}}$ and $\Delta_{48\ \mathrm{CDES}\ 90}$ values used to calculate this regression can be found in Table 6. Of the 21 carbonates in Figure 11, all lie within 1 SE of the 95 % confidence interval of the regression, with the exception of Merck, Carmel Chalk, and 47407 Coral.

The 47407 Coral was the only sample for which we determined a $\Delta_{48\ \mathrm{CDES}\ 90}$ value and did not include it in the regression due to the apparent offset from equilibrium. 47407 Coral is a deep-sea coral of the genus *Desmophyllum* with an estimated growth temperature of 4.2 °C.[59] Guo et al.[27] used model estimates to predict a negative correlation between Δ_{47} and Δ_{48} values for cold-water corals, with kinetic effects causing enrichments in Δ_{47} values and depletions in Δ_{48}

values. Using the framework proposed by Tripati et al.[5] and developed by Guo et al.[27] and Bajnai et al.[12], we determined that the 47407 Coral exhibits an enrichment of 0.030 ‰ in Δ_{47} and depletion of -0.018 ‰ in Δ_{48}. Nominal equilibrium was defined by the temperature-dependent regression through the remaining carbonates, and the offsets were determined by using a kinetic slope for CO_2 absorption in corals of -0.6[12,27]. Bajnai et al.[12] also measured Δ_{47} and Δ_{48} values for a coral of the same genus (*Desmophyllum*) and a brachiopod (*Magellania venosa*) and observed similar enrichments in Δ_{47} (0.038 ‰ to 0.069 ‰) and depletions in Δ_{48} (-0.0004 ‰ to -0.095 ‰). Additionally, modeling from Guo et al.[27] and Bajnai et al.[12] predicts deviations from equilibrium of a similar magnitude.

3.6.a Comparison of experimentally determined Δ_{47} and Δ_{48} regressions

We compared the experimental Δ_{47} and Δ_{48} regressions determined here (Equation 9) to those from Swart et al.[13] and Fiebig et al.[14] using a sum-of-squares F test (Supplementary Table S23). This compares the fit of a regression through all datasets to the fit of individual regressions for each dataset, and this tests whether the datasets differ sufficiently from each other to warrant separate regressions. The error associated with each regression is derived from the SE of its respective sample and how well the data are represented by the regression. The error from individual regressions is compared to the total error for the combined regression. The dataset from this study contains 20 carbonates, including standards and Devils Hole calcite. The dataset from Swart et al.[13] contains 7 inorganic precipitations in 5 ^{o}C increments from 5 ^{o}C to 65 ^{o}C and carbonate standards ETH-1, ETH-2, ETH-3, and ETH-4. The dataset from Fiebig et al.[14] includes 16 total carbonate samples, some of which are combined into averages yielding 10 samples that are used for comparison here, including lake calcite, Devils Hole calcite, inorganic calcite precipitations, and calcite equilibrated at high temperatures, with crystallization temperatures for all samples ranging from 8 ^{o}C to 1100 ^{o}C. We found no evidence of statistically significant differences between the individual regressions ($F = 0.43$; $p = 0.86$), and we therefore elected to use a combined regression (Figure 11b), described by Equation 10, which is composed of 41 carbonates.

Equation 10

$$\Delta_{48\ CDES\ 90} = (0.1132 \pm 0.010) + (0.008 \pm 0.055)\ \Delta_{47\ CDES\ 90} + (0.3692 \pm 0.065)\ \Delta_{47\ CDES\ 90}{}^2$$

3.7 Comparison of Devils Hole Δ_{47} and Δ_{48}

We analyzed 4 Devils Hole samples from core DH-2 for paired Δ_{47} and Δ_{48} values, including DH-10 (172 ± 4 ka), DH-11 (163 ± 5 ka), DH-12 (57 ± 5 ka), and DH-13 (151 ± 4 ka)[29] (Figure 12, Table 7), that previously were measured for Δ_{47} in Tripati et al.[5]. The samples were re-analyzed on the Nu Perspective mass spectrometers and standardized using carbonate-based standardization. Final Δ_{47} and Δ_{48} values were compared using an ANOVA followed by adjustment for multiple comparisons using a Tukey's Honest Significant Difference post-hoc test. The Δ_{48} replicate-level data from this study were statistically indistinguishable from the Δ_{48} replicate-level data from Fiebig et al.[14] ($q = 0.45$; $p = 0.99$) and Bajnai et al.[33] ($q = 0.17$; $p = 0.99$) produced using carbonate-based standardization, but significantly different from the replicate-level data from Bajnai et al.[33] ($q = 4.81$; $p = 0.0042$) calculated with gas-based standardization (Supplementary Table 20). The Δ_{47} replicate-level data from this study were significantly different from the Δ_{47} replicate-level data in Bajnai et al.[33] ($q = 4.54$; $p = 0.0044$) and Fiebig et al.[14] ($q = 4.75$; $p = 0.0027$). The mean differences between values from this study and Bajnai et al.[33] is 0.008 ‰, and 0.012 ‰ from Fiebig et al.[14] We cannot preclude the possibility there are small, yet resolvable differences in Devils Hole clumped isotope values from samples of different ages, given that we did not measure the same samples (Table 7). It is also possible they may arise from small differences in standardization procedures used between studies.

3.8 Regression-form acid digestion fractionation factors, $\Delta^*_{63\text{-}47}$ and $\Delta^*_{64\text{-}48}$

Model calculations from Guo et al.[3] predicted that acid digestion fractionation factors (AFFs) for when calcite mineral is digested in phosphoric acid, $\Delta^*_{63\text{-}47}$ and $\Delta^*_{64\text{-}48}$, should depend on the Δ_{63} and Δ_{64} values of the reactant carbonate, respectively. Here, to calculate this dependence, nonlinear regressions of the theoretical model equilibrium Δ_{63} or Δ_{64} and temperature[4,5] were used to determine theoretical equilibrium Δ_{63} and Δ_{64} values for the precipitation temperature of Devils Hole mammillary calcite at 33.7 °C[29] ($\Delta_{63} \approx 0.3707$ ‰; $\Delta_{64} \approx 0.1092$ ‰) and ETH-1 and ETH-2 at 600 °C[56] ($\Delta_{63} \approx 0.0179$ ‰; $\Delta_{64} \approx 0.0022$ ‰). The experimentally determined $\Delta_{47\ \text{I-CDES}}$ and $\Delta_{48\ \text{CDES 90}}$ values for DH-2 average and the pooled average of ETH-1 and ETH-2 were subtracted from the model equilibrium Δ_{63} and Δ_{64} values, respectively, to yield AFFs for calcite at 33.7 °C ($\Delta^*_{63\text{-}47} = 0.1949$ ‰; $\Delta^*_{64\text{-}48} = 0.1308$ ‰) and 600 °C ($\Delta^*_{63\text{-}47} = 0.1881$ ‰; $\Delta^*_{64\text{-}48} = 0.1300$ ‰) using Equations 11 and 12

$$\Delta^*_{63\text{-}47} = \Delta_{47\ \text{I-CDES}} - \Delta_{63} \qquad \text{Equation 11}$$

$$\Delta^*_{63\text{-}47} = \Delta_{48\ \text{CDES 90}} - \Delta_{64} \qquad \text{Equation 12}$$

where $\Delta^*_{63\text{-}47}$ and $\Delta^*_{63\text{-}47}$ are the AFFs. Devils Hole calcite was used in construction of the coupled carbonate clumped isotope relationship because it is assumed to have precipitated near isotopic equilibrium due to extremely slow precipitation rate (0.1-0.8 µm year-1), low calcite saturation index (0.16-0.21) and a stable temperature of 33.7 (±0.8) °C throughout the Holocene.[29,30,60] The pooled average of ETH-1 and ETH-2 was used because their $\Delta_{47\ \text{I-CDES}}$ and $\Delta_{48\ \text{CDES 90}}$ values were statistically indistinguishable, and both have a known equilibration temperature of 600 °C.[56] Additionally, samples equilibrated at high temperatures are much less likely to have detectable kinetic biases due to faster exchange of isotopes among isotopologues and decreased time to reach isotopic equilibrium.

Linear regressions were made using $\Delta^*_{63\text{-}47}$ versus Δ_{63}, and $\Delta^*_{64\text{-}48}$ versus Δ_{64} for DH-2 average (33.7 °C) and the pooled average of ETH-1 and ETH-2 (600 °C) (Figure 13 a,b). The slope and intercept from these regressions were used to calculate $\Delta^*_{63\text{-}47}$ and $\Delta^*_{64\text{-}48}$ for 0-1000 °C (Table 8), using Equations 13 and 14.

$$\Delta^*_{63\text{-}47} = 0.0193 \times \Delta_{63} + 0.1878 \qquad \text{Equation 13}$$

$$\Delta^*_{64\text{-}48} = 0.0077 \times \Delta_{64} + 0.1300 \qquad \text{Equation 14}$$

The relationship between precipitation temperature and $\Delta^*_{63\text{-}47}$ from 0-600 °C (Figure 13c) is represented by Equation 14 ($r^2 = 1$). The relationship between precipitation temperature and $\Delta^*_{64\text{-}48}$ from 0-300 °C (Figure 13d) is represented by Equation 15 ($r^2 = 1$), and 300-1000 °C (Figure 13e) is represented by Equation 16 ($r^2 = 1$). Equations 15-17 use temperature in degrees Celsius.

Equation 15

$$\Delta^*_{63\text{-}47} = [0.1968 \pm (1.805 \times 10^{-5})] - [(6.111 \times 10^{-5}) \pm (5.894 \times 10^{-7})]T + [(1.922 \times 10^{-7}) \pm (4.733 \times 10^{-9})]T^2 - [(2.965 \times 10^{-10}) \pm (1.304 \times 10^{-11})]T^3 + [(1.762 \times 10^{-13}) \pm (1.126 \times 10^{-14})]T^4$$

Equation 16

$$\Delta^*_{64\text{-}48} = [0.1312 \pm (7.348 \times 10^{-7})] - [(1.266 \times 10^{-5}) \pm (4.736 \times 10^{-8})]T + [(6.890 \times 10^{-8}) \pm (8.299 \text{ x } 10^{-10})]T^2 - [(2.029 \times 10^{-10}) \pm (4{,}756 \times 10^{-12})]T^3 + [(2.428 \times 10^{-13}) \pm (8.335 \times 10^{-15})]T^4$$

Equation 17

$$\Delta^*_{64\text{-}48} = [0.1305 \pm (2.101 \times 10^{-5})] - [(2.165 \text{ x } 10^{-6}) \pm (1.516 \times 10^{-7})]T + [(4.011 \times 10^{-9}) \pm (3.858 \times 10^{-10})]T^2 - [(3.377 \times 10^{-12}) \pm (4.135 \times 10^{-13})]T^3 + [(1.072 \times 10^{-15}) \pm (1.587 \times 10^{-16})]T^4$$

The relationship between $\Delta^*_{63\text{-}47}$ and $\Delta^*_{64\text{-}48}$ is represented by Equation 18.

$$\Delta^*_{64\text{-}48} = (0.3964 \pm 0.0033) + (-2.898 \pm 0.0340)\,\Delta^*_{63\text{-}47} + (7.88 \pm 0.0887)\,\Delta^{*2}_{63\text{-}47} \qquad \text{Equation 18}$$

For samples with unknown precipitation temperature, $\Delta^*_{63\text{-}47}$ and $\Delta^*_{64\text{-}48}$ can be calculated using Equations 19 and 20 (Figure 14a, b).

$$\Delta^*_{63\text{-}47} = 0.0190 \times \Delta_{47\ \text{I-CDES}} + 0.1842 \qquad \text{Equation 19}$$

$\Delta^*_{64\text{-}48} = 0.0077 \times \Delta_{48\ \mathrm{CDES}\ 90} + 0.1290$ Equation 20

where $\Delta_{47\ \mathrm{I\text{-}CDES}}$ and $\Delta_{48\ \mathrm{CDES}\ 90}$ are values experimentally determined. Equations 21 and 22 may be used to calculate Δ_{63} and Δ_{64} from $\Delta_{47\ \mathrm{I\text{-}CDES}}$ and $\Delta_{48\ \mathrm{CDES}\ 90}$ values (Figure 14c, d).

Equation 21

$\Delta^*_{63\text{-}47} = (-0.1845 \pm 0.0007) + (0.9839 \pm 0.0078)\Delta_{47\ \mathrm{I\text{-}CDES}} + (-0.0121 \pm 0.0299)\Delta_{47\ \mathrm{I\text{-}CDES}}^2 + (0.0207 \pm 0.0483)\ \Delta_{47\ \mathrm{I\text{-}CDES}}^3 + (-0.0125 \pm 0.0281)\Delta_{47\ \mathrm{I\text{-}CDES}}^4$

Equation 22

$\Delta_{64} = (-0.1377 \pm 0.0048) + (1.166 \pm 0.0981)\Delta_{48\ \mathrm{CDES}\ 90} + (-1.267 \pm 0.7306)\Delta_{488\ \mathrm{CDES}\ 90}^2 + (4.007 \pm 2.363)\Delta_{48\ \mathrm{CDES}\ 90}^3 + (-4.645 \pm 2.807)\Delta_{488\ \mathrm{CDES}\ 90}^4$

where $\Delta_{47\ \mathrm{I\text{-}CDES}}$ and $\Delta_{48\ \mathrm{CDES}\ 90}$ values are experimentally determined values.

The $\Delta^*_{63\text{-}47}$ and Δ_{63} slope of 0.0193 determined here (Figure 13a) differs by -0.0112 ‰ from the model predicted slope from Guo et al.[3] of 0.0305. The model calculated the dependence based on carbonates with □^{13}C = 0 and □^{18}O = 0, however, this may not be the source of the offset because the slope is only predicted to change by ~0.002 ‰ and ~-0.0005 ‰ for a 50 ‰ increase in □^{13}C and □^{18}O, respectively.[3] The slope offset may in-part arise from approximations made in the model calculations for isotopologues containing ^{17}O, and uncertainty in the slope determined in this study from the use of only two temperatures.

Fiebig et al.[7] used a similar method to determine AFFs at 600 ^{o}C. Our 600 ^{o}C $\Delta^*_{63\text{-}47}$ and $\Delta^*_{64\text{-}48}$ values differed by 0.008 ‰ and 0.006 ‰, respectively, from their 600 ^{o}C $\Delta^*_{63\text{-}47}$ and $\Delta^*_{64\text{-}48}$ values of 0.196 ‰ and 0.136 ‰. Because the calculation of AFFs relies on the long term ETH-1 and ETH-2 Δ_{47} and Δ_{48} values, the difference in AFFs is equivalent to the difference in the long term pooled average ETH-1 and ETH-2 Δ_{47} and Δ_{48} values from this study (pooled average ETH-1 and ETH-2 $\Delta_{47\ \mathrm{I\text{-}CDES}} = 0.206 \pm 0.0006$ ‰, n = 1497; $\Delta_{48\ \mathrm{CDES}\ 90} = 0.132 \pm 0.002$ ‰, n = 903) versus Fiebig et al.[7] (pooled average ETH-1 and ETH-2 $\Delta_{47\ \mathrm{I\text{-}CDES}} = 0.214 \pm 0.005$ ‰, n = 37; $\Delta_{48\ \mathrm{CDES}\ 90} = 0.138 \pm 0.015$ ‰, n = 37).

3.9 Temperature-dependent Δ_{47} and Δ_{48} equilibrium combining theory and experimental values

Temperature-dependent $\Delta_{47\ \mathrm{I\text{-}CDES}}$ and $\Delta_{48\ \mathrm{CDES}\ 90}$ equilibrium, referred to as $\Delta_{47\ \mathrm{I\text{-}CDES\ EQ}}$ and $\Delta_{48\ \mathrm{CDES\ 90\ EQ}}$, were calculated using equilibrium values predicted by theory from Hill et al.[4] and Tripati et al.[5] and combined with experimentally determined $\Delta_{47\ \mathrm{I\text{-}CDES}}$ and $\Delta_{48\ \mathrm{CDES}\ 90}$ values, with the AFFs described in Section 3.5. $\Delta_{47\ \mathrm{I\text{-}CDES\ EQ}}$ and $\Delta_{48\ \mathrm{CDES\ 90\ EQ}}$ were calculated using Equations 23 and 24 (Table 7)

$\Delta_{47\ \mathrm{I\text{-}CDES\ EQ}} = \Delta_{63} + \Delta^*_{63\text{-}47}$ Equation 23

$\Delta_{48\ \text{CDES 90 EQ}} = \Delta_{64} + \Delta^*_{64\text{-}48}$ Equation 24

where $\Delta^*_{63\text{-}47}$ and $\Delta^*_{64\text{-}48}$ values are those determined in Section 3.5. The $\Delta_{47\ \text{I-CDES EQ}}$ and $\Delta_{48\ \text{CDES 90 EQ}}$ equilibrium relationship (Figure 11a) is given by a second-degree polynomial in Equation 25.

$\Delta_{48\ \text{CDES 90 EQ}} = 0.1123 + 0.01971\ \Delta_{47\ \text{I-CDES EQ}} + 0.364(\Delta_{47\ \text{I-CDES EQ}})^2$ Equation 25

The temperature-dependent equilibrium relationships are described by Equations 26 and 27,

Equation 26

$\Delta_{47\ \text{I-CDES EQ}} = [0.6646 \pm (0.0009)] - [0.0032 \pm (3.033 \text{ x } 10^{-5})]T + [(1.012 \text{ x } 10^{-5}) \pm (2.449 \times 10^{-7})]T^2 - [(1.559 \times 10^{-8}) \pm (6.717 \times 10^{-10})]T^3 + [(9.251 \times 10^{-12}) \pm (5.802 \times 10^{-13})]T^4$

Equation 27

$\Delta_{48\ \text{CDES 90 EQ}} = [0.2842 \pm (0.0009)] - [0.0014 \pm (3.048 \times 10^{-5})]\text{T} + [(5.741 \times 10^{-6}) \pm (2.437 \times 10^{-7})]T^2 - [(1.017 \times 10^{-8}) \pm (6.749 \times 10^{-10})]T^3 + [(6.570 \times 10^{-12}) \pm (5.830 \times 10^{-13})]T^4$

where the temperature is Celsius.

The regression determined here using experimental Δ_{47} and Δ_{48} values for 20 carbonates, and the regression determined here using calcite mineral equilibrium theory with experimental AFFs, are statistically indistinguishable (F = 0.1157; p = 0.99) from the experimental Δ_{47} and Δ_{48} regressions determined in Fiebig et al.[14] and Swart et al.[13]

3.9.a Comparison of Δ_{48} and Δ_{47} equilibrium regressions using constant and regression-form AFFs with experimentally determined equilibrium regressions

To further constrain the Δ_{47} and Δ_{48} equilibrium relationship and quantify the effects of using a regression-form AFF or a constant AFF for $\Delta^*_{63\text{-}47}$ and $\Delta^*_{64\text{-}48}$ values, we have compared our Δ_{47} and Δ_{48} equilibrium regressions in Equation 23 (derived from theory and a regression-form AFF) and Equation 9 (derived from experimental data) to equilibrium regressions determined using constant AFFs.

Using the method described in Section 3.8, we determined the constant $\Delta^*_{63\text{-}47}$ and $\Delta^*_{64\text{-}48}$ values at 600 °C to be 0.1881 ‰ and 0.1300 ‰, respectively. This same method was used to calculate constant $\Delta^*_{63\text{-}47}$ and $\Delta^*_{64\text{-}48}$ values at 33.7 °C, which were determined to be 0.1949 ‰ and 0.1308 ‰, respectively. Equations 21 and 22 were then used to calculate $\Delta_{47\ \text{I-CDES EQ}}$ and Δ_{48}

CDES 90 EQ. The use of a constant AFF may introduce some uncertainties when extrapolating due to the compositional dependence of $\Delta^*_{63\text{-}47}$ and $\Delta^*_{64\text{-}48}$ values on the Δ_{63} and Δ_{64} values of the carbonate mineral.[3] This is supported by the comparison of equilibrium regressions calculated using low temperature (33.7 °C), high temperature (600 °C), and regression-form AFFs (Figure 15). The regressions calculated using constant AFFs determined at 600 °C have a $\Delta_{47\text{ I-CDES}}$ offset of ~0.007 ‰ when extrapolated to low temperatures. The opposite is true for equilibrium regressions using a constant AFF determined at 33.7 °C, which have a $\Delta_{47\text{ I-CDES}}$ offset of ~0.007 ‰ when extrapolated to high temperatures. Experimental $\Delta_{47\text{ I-CDES}}$ data for low and high temperatures is better represented using a regression-form AFF.

The range for Δ_{48} is compressed relative to Δ_{47}, and this contributes to smaller effects in Δ_{48} when extrapolating AFFs. The regressions determined using low temperature and high temperature constant AFFs differ by ~0.0008 ‰ when extrapolated.

The equilibrium regression from Bajnai et al.[12] has a significant offset from the equilibrium regression determined in Swart et al.[13], Fiebig et al.[14], and here. In the 0-40 °C range, offsets in $\Delta_{47\text{ I-CDES 90 EQ}}$ and $\Delta_{48\text{ CDES 90 EQ}}$ between this study and Bajnai et al.[12] are 0.009 ‰ and 0.014 ‰, respectively, are equivalent to the measured difference in the Devils Hole calcite values from the two studies. Additional offsets may arise from anchor standard Δ_{47} values from this study being in the I-CDES[11] reference frame, while they use CDES 90. The Δ_{48} values from both studies use the CDES 90 reference frame with slightly different anchor standard values.

4. CONCLUSIONS

This study, which contains 5,461 Δ_{47} and 3,400 Δ_{48} measurements of carbonates, supports previous Δ_{47} research[10,11,31,56] that carbonate-based standardization is a robust technique. We show this approach provides reproducible data across multiple mass spectrometer configurations and demonstrate that carbonate-based standardization also produces statistically indistinguishable Δ_{48} data on varying instrumentation. Interlaboratory reproducibility of Δ_{48} values would likely be improved by the universal application of carbonate-based standardization using agreed upon carbonate standard values. We believe this is demonstrated by the Δ_{48} data produced here. We also show that a kernel density-based approach for data analysis can be used for clumped isotopes and provide an R script for its implementation. This method is statistically rigorous, minimizes the risk of unintentionally introducing human error or bias, and is reproducible.

We have constructed a temperature-dependent Δ_{47} and Δ_{48} equilibrium regression based on theory[4,5] and experimental AFFs, and an experimental Δ_{47} and Δ_{48} regression based on values for 20 carbonates including standards and Devils Hole. The experimental Δ_{47} and Δ_{48} regressions from this study, Fiebig et al.[14], and Swart et al.[13] are statistically indistinguishable, and a combined experimental regression was determined using these datasets.

Previous theoretical predictions from Guo et al.[3] hypothesized there may be a dependence of the acid digestion fractionation factors (AFFs), $\Delta^*_{63\text{-}47}$ and $\Delta^*_{64\text{-}48}$, on calcite mineral Δ_{63} and Δ_{64}. To constrain this dependence experimentally, we calculated AFFs using constants at low and high temperature, and a regression-form AFF. The Δ_{47} and Δ_{48} equilibrium regression using a regression-form AFF had the best agreement with experimental regressions, and did not have offsets when extrapolated, in contrast to regressions using constant AFFs.

Data Accessibility Statement

All code and raw data used in analyses are available for review at https://github.com/Tripati-Lab/Lucarelli-et-al. Upon acceptance for publication, code and raw data will be permanently archived at Dryad, a static link provided in the manuscript, and this section updated.

Acknowledgements

We thank laboratory members past and present for their work running standards, efforts in data entry, and contributions to discussions. This work was funded by DOE BES grant DE-FG02-13ER16402. HMC was supported through a postdoctoral fellowship by the Institutional Research and Academic Career Development Awards (IRACDA) program at UCLA (Award # K12 GM106996).

References

1. Schauble, E. A., Ghosh, P. & Eiler, J. M. Preferential formation of 13C–18O bonds in carbonate minerals, estimated using first-principles lattice dynamics. *Geochimica et Cosmochimica Acta* **70**, 2510–2529 (2006). https://doi.org/10.1016/j.gca.2006.02.011.
2. Ghosh, P. *et al.* 13C–18O bonds in carbonate minerals: A new kind of paleothermometer. *Geochimica et Cosmochimica Acta* **70**, 1439–1456 (2006). https://doi.org/10.1016/j.gca.2005.11.014.
3. Guo, W., Mosenfelder, J. L., Goddard, W. A. & Eiler, J. M. Isotopic fractionations associated with phosphoric acid digestion of carbonate minerals: Insights from first-principles theoretical modeling and clumped isotope measurements. *Geochimica et Cosmochimica Acta* **73**, 7203–7225 (2009). https://doi.org/10.1016/j.gca.2009.05.071.
4. Hill, P. S., Tripati, A. K. & Schauble, E. A. Theoretical constraints on the effects of pH, salinity, and temperature on clumped isotope signatures of dissolved inorganic carbon species and precipitating carbonate minerals. *Geochimica et Cosmochimica Acta* **125**, 610–652 (2014). https://doi.org/10.1016/j.gca.2013.06.018.
5. Tripati, A. K. *et al.* Beyond temperature: Clumped isotope signatures in dissolved inorganic carbon species and the influence of solution chemistry on carbonate mineral composition. *Geochimica et Cosmochimica Acta* **166**, 344–371 (2015). https://doi.org/10.1016/j.gca.2015.06.021.

6. Guo, Y., Deng, W. & Wei, G. Kinetic effects during the experimental transition of aragonite to calcite in aqueous solution: Insights from clumped and oxygen isotope signatures. *Geochimica et Cosmochimica Acta* **248**, 210–230 (2019). https://doi.org/10.1016/j.gca.2019.01.012.
7. Fiebig, J. *et al.* Combined high-precision Δ48 and Δ47 analysis of carbonates. *Chemical Geology* **522**, 186–191 (2019). https://doi.org/10.1016/j.chemgeo.2019.05.019.
8. Eiler, J. M. & Schauble, E. 18O13C16O in Earth's atmosphere. *Geochimica et Cosmochimica Acta* **68**, 4767–4777 (2004). https://doi.org/10.1016/j.gca.2004.05.035.
9. Eiler, J. M. "Clumped-isotope" geochemistry—The study of naturally-occurring, multiply-substituted isotopologues. *Earth and Planetary Science Letters* **262**, 309–327 (2007). https://doi.org/10.1016/j.epsl.2007.08.020.
10. Dennis, K. J., Affek, H. P., Passey, B. H., Schrag, D. P. & Eiler, J. M. Defining an absolute reference frame for 'clumped' isotope studies of CO2. *Geochimica et Cosmochimica Acta* **75**, 7117–7131 (2011). https://doi.org/10.1016/j.gca.2011.09.025.
11. Bernasconi, S. M. *et al.* InterCarb: A Community Effort to Improve Interlaboratory Standardization of the Carbonate Clumped Isotope Thermometer Using Carbonate Standards. *Geochem Geophys Geosyst* **22**, (2021). https://doi.org/10.1029/2020GC009588.
12. Bajnai, D. *et al.* Dual clumped isotope thermometry resolves kinetic biases in carbonate formation temperatures. *Nat Commun* **11**, 4005 (2020). https://doi.org/10.1038/s41467-020-17501-0.
13. Swart, P. K. *et al.* A calibration equation between Δ_{48} values of carbonate and temperature. *Rapid Commun Mass Spectrom* **35**, (2021). https://doi.org/10.1002/rcm.9147.
14. Fiebig, J. *et al.* Calibration of the dual clumped isotope thermometer for carbonates. *Geochimica et Cosmochimica Acta* S0016703721004208 (2021) doi:10.1016/j.gca.2021.07.012. https://doi.org/10.1016/j.gca.2021.07.012.
15. Urey, H. C. The thermodynamic properties of isotopic substances. *J. Chem. Soc.* 562 (1947) doi:10.1039/jr9470000562. https://doi.org/10.1039/jr9470000562.
16. Passey, B. H. & Henkes, G. A. Carbonate clumped isotope bond reordering and geospeedometry. *Earth and Planetary Science Letters* **351–352**, 223–236 (2012). https://doi.org/10.1016/j.epsl.2012.07.021.
17. Tripati, A. K. *et al.* 13C–18O isotope signatures and 'clumped isotope' thermometry in foraminifera and coccoliths. *Geochimica et Cosmochimica Acta* **74**, 5697–5717 (2010). https://doi.org/10.1016/j.gca.2010.07.006.
18. Henkes, G. A. *et al.* Temperature evolution and the oxygen isotope composition of Phanerozoic oceans from carbonate clumped isotope thermometry. *Earth and Planetary Science Letters* **490**, 40–50 (2018). https://doi.org/10.1016/j.epsl.2018.02.001.
19. Huntington, K. W., Wernicke, B. P. & Eiler, J. M. Influence of climate change and uplift on Colorado Plateau paleotemperatures from carbonate clumped isotope thermometry. *Tectonics* **29**, 2009TC002449 (2010). https://doi.org/10.1029/2009TC002449.

20. Lechler, A. R., Niemi, N. A., Hren, M. T. & Lohmann, K. C. Paleoelevation estimates for the northern and central proto-Basin and Range from carbonate clumped isotope thermometry: Δ_{47} PALEOALTIMETRY OF BASIN AND RANGE. *Tectonics* **32**, 295–316 (2013). https://doi.org/10.1002/tect.20016.
21. Eagle, R. A. *et al.* Body temperatures of modern and extinct vertebrates from 13C-18O bond abundances in bioapatite. *Proceedings of the National Academy of Sciences* **107**, 10377–10382 (2010). https://doi.org/10.1073/pnas.0911115107.
22. Affek, H. P., Bar-Matthews, M., Ayalon, A., Matthews, A. & Eiler, J. M. Glacial/interglacial temperature variations in Soreq cave speleothems as recorded by 'clumped isotope' thermometry. *Geochimica et Cosmochimica Acta* **72**, 5351–5360 (2008). https://doi.org/10.1016/j.gca.2008.06.031.
23. Lloyd, M. K., Eiler, J. M. & Nabelek, P. I. Clumped isotope thermometry of calcite and dolomite in a contact metamorphic environment. *Geochimica et Cosmochimica Acta* **197**, 323–344 (2017). https://doi.org/10.1016/j.gca.2016.10.037.
24. Daëron, M. *et al.* Most Earth-surface calcites precipitate out of isotopic equilibrium. *Nat Commun* **10**, 429 (2019). https://doi.org/10.1038/s41467-019-08336-5.
25. Kimball, J., Eagle, R. & Dunbar, R. Carbonate "clumped" isotope signatures in aragonitic scleractinian and calcitic gorgonian deep-sea corals. *Biogeosciences* **13**, 6487–6505 (2016). https://doi.org/10.5194/bg-13-6487-2016.
26. Saenger, C. *et al.* Carbonate clumped isotope variability in shallow water corals: Temperature dependence and growth-related vital effects. *Geochimica et Cosmochimica Acta* **99**, 224–242 (2012). https://doi.org/10.1016/j.gca.2012.09.035.
27. Guo, W. Kinetic clumped isotope fractionation in the DIC-H2O-CO2 system: Patterns, controls, and implications. *Geochimica et Cosmochimica Acta* **268**, 230–257 (2020). https://doi.org/10.1016/j.gca.2019.07.055.
28. Hill, P. S., Schauble, E. A. & Tripati, A. Theoretical constraints on the effects of added cations on clumped, oxygen, and carbon isotope signatures of dissolved inorganic carbon species and minerals. *Geochimica et Cosmochimica Acta* **269**, 496–539 (2020). https://doi.org/10.1016/j.gca.2019.10.016.
29. Winograd, I. J. *et al.* Continuous 500,000-Year Climate Record from Vein Calcite in Devils Hole, Nevada. *Science* **258**, 255–260 (1992). https://doi.org/10.1016/j.yqres.2006.06.003.
30. Coplen, T. B. Calibration of the calcite–water oxygen-isotope geothermometer at Devils Hole, Nevada, a natural laboratory. *Geochimica et Cosmochimica Acta* **71**, 3948–3957 (2007). https://doi.org/10.1016/j.gca.2007.05.028.
31. Upadhyay, D. *et al.* Carbonate clumped isotope analysis (Δ_{47}) of 21 carbonate standards determined via gas-source isotope-ratio mass spectrometry on four instrumental configurations using carbonate-based standardization and multiyear data sets. *Rapid Commun Mass Spectrom* **35**, (2021).
32. Defliese, W. F. & Tripati, A. Analytical effects on clumped isotope thermometry: Comparison of a common sample set analyzed using multiple instruments, types of

standards, and standardization windows. *Rapid Commun Mass Spectrom* **34**, (2020). https://doi.org/10.1002/rcm.8666.

33. Bajnai, D. *et al.* Devils Hole Calcite Was Precipitated at ±1°C Stable Aquifer Temperatures During the Last Half Million Years. *Geophys Res Lett* **48**, (2021). https://doi.org/10.1029/2021GL093257.
34. Winograd, I. J., Coplen, T. B., Szabo, B. J. & Riggs, A. C. A 250,000-Year Climatic Record from Great Basin Vein Calcite: Implications for Milankovitch Theory. *Science* **242**, 1275–1280 (1988). https://doi.org/10.1126/science.242.4883.1275.
35. Kluge, T., Affek, H. P., Dublyansky, Y. & Spötl, C. Devils Hole paleotemperatures and implications for oxygen isotope equilibrium fractionation. *Earth and Planetary Science Letters* **400**, 251–260 (2014). https://doi.org/10.1016/j.epsl.2014.05.047.
36. Passey, B. H., Levin, N. E., Cerling, T. E., Brown, F. H. & Eiler, J. M. High-temperature environments of human evolution in East Africa based on bond ordering in paleosol carbonates. *Proceedings of the National Academy of Sciences* **107**, 11245–11249 (2010). https://doi.org/10.1073/pnas.1001824107.
37. John, C. M. & Bowen, D. Community software for challenging isotope analysis: First applications of 'Easotope' to clumped isotopes: Community software for challenging isotope analysis. *Rapid Commun. Mass Spectrom.* **30**, 2285–2300 (2016). https://doi.org/10.1002/rcm.7720.
38. Brand, W. A., Assonov, S. S. & Coplen, T. B. Correction for the 17O interference in δ(13C) measurements when analyzing CO2 with stable isotope mass spectrometry (IUPAC Technical Report). *Pure and Applied Chemistry* **82**, 1719–1733 (2010). https://doi.org/10.1351/PAC-REP-09-01-05.
39. Daëron, M., Blamart, D., Peral, M. & Affek, H. P. Absolute isotopic abundance ratios and the accuracy of Δ47 measurements. *Chemical Geology* **442**, 83–96 (2016). https://doi.org/10.1016/j.chemgeo.2016.08.014.
40. Huntington, K. W. *et al.* Methods and limitations of 'clumped' CO_2 isotope (Δ_{47}) analysis by gas-source isotope ratio mass spectrometry. *J. Mass Spectrom.* **44**, 1318–1329 (2009). https://doi.org/10.1002/jms.1614.
41. Wang, Z., Schauble, E. A. & Eiler, J. M. Equilibrium thermodynamics of multiply substituted isotopologues of molecular gases. *Geochimica et Cosmochimica Acta* **68**, 4779–4797 (2004). https://doi.org/10.1016/j.gca.2004.05.039.
42. Daëron, M. Full Propagation of Analytical Uncertainties in Δ_{47} Measurements. *Geochem Geophys Geosyst* **22**, (2021). https://doi.org/10.1029/2020GC009592.
43. Zaarur, S., Affek, H. P. & Brandon, M. T. A revised calibration of the clumped isotope thermometer. *Earth and Planetary Science Letters* **382**, 47–57 (2013). https://doi.org/10.1016/j.epsl.2013.07.026.
44. Burgener, L. *et al.* Variations in soil carbonate formation and seasonal bias over >4 km of relief in the western Andes (30°S) revealed by clumped isotope thermometry. *Earth and Planetary Science Letters* **441**, 188–199 (2016). https://doi.org/10.1016/j.epsl.2016.02.033.

45. Peral, M. *et al.* Updated calibration of the clumped isotope thermometer in planktonic and benthic foraminifera. *Geochimica et Cosmochimica Acta* **239**, 1–16 (2018). https://doi.org/10.1016/j.gca.2018.07.016.
46. Meckler, A. N., Ziegler, M., Millán, M. I., Breitenbach, S. F. M. & Bernasconi, S. M. Long-term performance of the Kiel carbonate device with a new correction scheme for clumped isotope measurements: Performance and correction of Kiel clumped isotope measurements. *Rapid Commun. Mass Spectrom.* **28**, 1705–1715 (2014). https://doi.org/10.1002/rcm.6949.
47. Bonifacie, M. *et al.* Calibration of the dolomite clumped isotope thermometer from 25 to 350 °C, and implications for a universal calibration for all (Ca, Mg, Fe)CO3 carbonates. *Geochimica et Cosmochimica Acta* **200**, 255–279 (2017). https://doi.org/10.1016/j.gca.2016.11.028.
48. R Core Team. R: A language and environment for statistical computing. (2021). https://www.R-project.org/.
49. Correa-Quezada, R., Cueva-Rodríguez, L., Álvarez-García, J. & del Río-Rama, M. de la C. Application of the Kernel Density Function for the Analysis of Regional Growth and Convergence in the Service Sector through Productivity. *Mathematics* **8**, 1234 (2020). https://doi.org/10.3390/math8081234.
50. Seaman, D. E. & Powell, R. A. An Evaluation of the Accuracy of Kernel Density Estimators for Home Range Analysis. *Ecology* **77**, 2075–2085 (1996). https://doi.org/10.2307/2265701.
51. Pulkkinen, S. Nonlinear kernel density principal component analysis with application to climate data. *Stat Comput* **26**, 471–492 (2016). https://doi.org/10.1007/s11222-014-9539-0.
52. Wahiduzzaman, M. & Yeasmin, A. A kernel density estimation approach of North Indian Ocean tropical cyclone formation and the association with convective available potential energy and equivalent potential temperature. *Meteorol Atmos Phys* **132**, 603–612 (2020). https://doi.org/10.1007/s00703-019-00711-7.
53. Lee, W. J., Mendis, G. P., Triebe, M. J. & Sutherland, J. W. Monitoring of a machining process using kernel principal component analysis and kernel density estimation. *J Intell Manuf* **31**, 1175–1189 (2020). https://doi.org/10.1007/s10845-019-01504-w.
54. Sheather, S. J. & Jones, M. C. A Reliable Data-Based Bandwidth Selection Method for Kernel Density Estimation. *Journal of the Royal Statistical Society: Series B (Methodological)* **53**, 683–690 (1991). https://doi.org/10.1111/j.2517-6161.1991.tb01857.x.
55. Deng, H. & Wickham, H. Density estimation in R. (2011). https://vita.had.co.nz/papers/density-estimation.pdf.
56. Bernasconi, S. M. *et al.* Reducing Uncertainties in Carbonate Clumped Isotope Analysis Through Consistent Carbonate-Based Standardization. *Geochem. Geophys. Geosyst.* **19**, 2895–2914 (2018). https://doi.org/10.1029/2017GC007385.
57. J Pinheiro, Bates, D., DebRoy, S., Sarkar, D. & R Core Team. nlme: Linear and nonlinear mixed effects models. (2021). https://CRAN.R-project.org/package=nlme.
58. Lenth, R. V. emmeans: Estimated marginal means, aka least-squares means. (2021). https://CRAN.R-project.org/package=emmeans.

59. Thiagarajan, N., Adkins, J. & Eiler, J. Carbonate clumped isotope thermometry of deep-sea corals and implications for vital effects. *Geochimica et Cosmochimica Acta* **75**, 4416–4425 (2011). https://doi.org/10.1016/j.gca.2011.05.004.
60. Winograd, I. J. *et al.* Devils Hole, Nevada, δ^{18}O record extended to the mid-Holocene. *Quat. res.* **66**, 202–212 (2006). https://doi.org/10.1016/j.yqres.2006.06.003.

Figure Captions

Figure 1. Examples of relationships between δ^{47} and Δ_{47} values, and δ^{48} and Δ_{48} values, for different instrument configurations. **(A)** δ^{47} raw values vs Δ_{47} raw values on Nu Perspective-EG, (B) δ^{48} raw values vs Δ_{48} raw values for Nu Perspective-EG, **(C)** δ^{47} raw values vs Δ_{47} raw values on Nu Perspective-1, **(D)** δ^{48} raw values vs Δ_{48} raw values for Nu Perspective-1, **(E)** δ^{47} raw values vs Δ_{47} raw values on Nu Perspective-2, **(F)** δ^{48} raw values vs Δ_{48} raw values for Nu Perspective-2, (**G)** δ^{47} raw values vs Δ_{47} raw values on MAT 253, **(H)** δ^{48} raw values vs Δ_{48} raw values for MAT 253. The grey shading denotes that Δ_{48} values from MAT 253 were not included in the long-term combined instrument average. The slope is determined on a 10-day moving interval to account for instrument drift and applied to standards and samples as the slope correction. Nu Perspective-EG used 1000 ^{o}C and 25 ^{o}C equilibrated gases relative to the working gas composition, and Nu Perspective-1, Nu Perspective-2, and MAT 253 used ETH-1 and ETH-2 for the slope correction.

Figure 2. Examples of the slope and transfer function corrections applied to raw Δ_{47} values and Δ_{48} values using both equilibrated gas-based corrections and carbonate-based corrections. This figure is adapted from Dennis et al.[10]

Figure 3. Examples of relationships between slope corrected values and expected values for **A)** $\Delta_{47\ sc}$ and $\Delta_{47\ I\text{-}CDES}$ values on Nu Perspective-EG, **B)** $\Delta_{48\ sc}$ and $\Delta_{48\ CDES\ 90}$ values on Nu Perspective-EG, **C)** $\Delta_{47\ SC}$ and $\Delta_{47\ I\text{-}CDES}$ values on Nu Perspective-1, **D)** $\Delta_{48\ sc}$ and $\Delta_{48\ CDES\ 90}$ values from Nu Perspective-2. Expected Δ_{47} values for 25 ^{o}C and 1000 ^{o}C gases are from Wang et al.[41] Expected Δ_{47} values for ETH-1, ETH-2, and ETH-3 are from Bernasconi et al.[11] Expected Δ_{48} values for 25 ^{o}C and 1000 ^{o}C gases are from Fiebig et al.[7] Expected Δ_{48} values for ETH-1, ETH-2, ETH-3 and Veinstrom are from this study.

Figure 4. Flow chart outlining the quality assurance steps we employed for each standard reported in this study, using ETH-1 $\Delta_{47\ I\text{-}CDES}$ from Nu Perspective-2 as an example.

Figure 5. Example of raw data throughout the quality control process. In all panels, the dashed vertical line represents the mean. **A)** Histogram of the raw replicate pool (N = 389); **B)** Density plot with histogram of the raw replicate pool and first recommended exclusions (solid vertical lines); **C)** Density plot of the replicate pool following initial exclusions using the nearest minima method (N = 378). Potential cutoff at 3σ (solid vertical lines) is shown; **D)** Histogram of the final replicate pool following a 3σ exclusion (mean = 0.1327 ‰, SD = 0.065, N = 376). Note that the x and y axis scales differ between plots**. E)** Density plot of the replicate pool following initial exclusions using the nearest minima method (N = 378). Potential cutoff at 5σ (solid vertical lines) is shown. **F)** Histogram of the final replicate pool following a 5σ exclusion (mean = 0.1327 ‰, SD = 0.066, n = 378). The difference in means in a 3σ versus 5σ cutoff is two orders

of magnitude smaller than the precision at which clumped isotope values are typically reported (absolute difference 0.000001 ‰).

Figure 6. Density curves for $\Delta_{47\ \mathrm{I\text{-}CDES}}$ values measured from the anchor standards ETH-1 and ETH-2, and non-anchor standards ETH-4 and Veinstrom on Nu-Perspective-1 (**A-D)**, Nu-Perspective-2 **(E-H)**, and MAT 253 **(I-L)**. In all plots, dashed vertical lines indicate the mean using a 3σ cutoff (purple) and 5σ cutoff (blue); these lines are too close together to be visually distinguished and so the mean values are reported in text. **A)** ETH-1 on Nu-Perspective-1. If using a 3σ cutoff, final mean = 0.2066 ‰, SD = 0.025, N = 85. If using a 5σ cutoff, final mean = 0.2076 ‰, SD = 0.026, N = 86. **B)** ETH-2 on Nu-Perspective-1. Regardless of whether a 3σ or 5σ cutoff is used, final mean = 0.2081 ‰, SD = 0.020, N = 69. **C)** ETH-4 on Nu-Perspective-1. Regardless of whether a 3σ or 5σ cutoff is used, final mean = 0.4552 ‰, SD = 0.020, N = 64. **D)** Veinstrom on Nu-Perspective-1. Regardless of whether a 3σ or 5σ cutoff is used, final mean = 0.6365 ‰, SD = 0.026, N = 102. **E)** ETH-1 on Nu-Perspective-2. If using a 3σ cutoff, final mean = 0.2053 ‰, SD = 0.026, N = 402. If using a 5σ cutoff, final mean = 0.2055 ‰, SD = 0.026, N = 403. **F)** ETH-2 on Nu-Perspective-2. If using a 3σ cutoff, final mean = 0.2060 ‰, SD = 0.026, N = 386. If using a 5σ cutoff, final mean = 0.2065 ‰, SD = 0.028, N =390. **G)** ETH-4 on Nu-Perspective-2. If using a 3σ cutoff, final mean = 0.4411 ‰, SD = 0.026, N = 191. If using a 5σ cutoff, final mean = 0.4420 ‰, SD = 0.027, N = 193. **H)** Veinstrom on Nu-Perspective-2. If using a 3σ cutoff, final mean = 0.6341 ‰, SD = 0.030, N = 322. If using a 5σ cutoff, final mean = 0.6338 ‰, SD = 0.030, N = 323. **I)** ETH-1 on MAT 253. Regardless of whether a 3σ or 5σ cutoff is used, final mean = 0.2063 ‰, SD = 0.020, N = 284. **J)** ETH-2 on MAT 253. If using a 3σ cutoff, final mean = 0.2066 ‰, SD = 0.024, N = 271. If using a 5σ cutoff, final mean = 0.2063 ‰, SD = 0.024, N = 272. **K)** ETH-4 on MAT 253. If using a 3σ cutoff, final mean = 0.4451 ‰, SD = 0.021, N = 208. If using a 5σ cutoff, final mean = 0.4448 ‰, SD = 0.021, N = 209. **L)** Veinstrom on MAT 253. If using a 3σ cutoff, final mean = 0.6315 ‰, SD = 0.022, N = 304. If using a 5σ cutoff, final mean = 0.6318 ‰, SD = 0.023, N = 305.

Figure 7. Density curves for $\Delta_{48\ \mathrm{CDES}\ 90}$ values measured from the anchor standards ETH-1 and ETH-2, and non-anchor standards ETH-4 and Veinstrom on Nu-Perspective-1 **(A-D)**, Nu-Perspective-2 **(E-H)**, and MAT 253 **(I-L)**. In all plots, dashed vertical lines indicate the mean using a 3σ cutoff (purple) and 5σ cutoff (blue); these lines are too close together to be visually distinguished and so the mean values are reported in text. **A)** ETH-1 on Nu-Perspective-1. Regardless of whether a 3σ or 5σ cutoff is used, final mean = 0.1301 ‰, SD = 0.051, N = 88. **B)** ETH-2 on Nu-Perspective-1. Regardless of whether a 3σ or 5σ cutoff is used, final mean = 0.1309 ‰, SD = 0.064, N = 73. **C)** ETH-4 on Nu-Perspective-1. Regardless of whether a 3σ or 5σ cutoff is used, final mean = 0.1975 ‰, SD = 0.059, N = 70. **D)** Veinstrom on Nu-Perspective-1. Regardless of whether a 3σ or 5σ cutoff is used, final mean = 0.2722 ‰, SD = 0.066, N = 100. **E)** ETH-1 on Nu-Perspective-2. If using a 3σ cutoff, final mean = 0.1327 ‰, SD = 0.065, N = 376. If using a 5σ cutoff, final mean = 0.1327 ‰, SD = 0.066, N = 378. **F)** ETH-2 on Nu-

Perspective-2. If using a 3σ cutoff, final mean = 0.1326 ‰, SD = 0.0563, N = 366. If using a 5σ cutoff, final mean = 0.1321 ‰, SD = 0.057, N = 367. **G)** ETH-4 on Nu-Perspective-2. Regardless of whether a 3σ or 5σ cutoff is used, final mean = 0.2028 ‰, SD = 0.058, N = 187. H) Veinstrom on Nu-Perspective-2. Regardless of whether a 3σ or 5σ cutoff is used, final mean = 0.2739 ‰, SD = 0.059, N = 336.

Figure 8. Final density distributions of the standards ETH-1, ETH-2, ETH-3, ETH-4, TV03, and Veinstrom, measured on multiple instrument configurations for $\Delta_{47\ \mathrm{I\text{-}CDES}}$ values **(A-F)** and $\Delta_{48\ \mathrm{CDES\ 90}}$ values **(G-L)**. We found no statistically significant differences in final values for each of the standards between any of the configurations. $\Delta_{48\ \mathrm{CDES\ 90}}$ values from MAT 253 are provided for informational purposes only and were not included in analyses. **A)** $\Delta_{47\ \mathrm{I\text{-}CDES}}$ values for ETH-1 on Nu Perspective-1, Nu Perspective-2, and MAT 253. **B)** $\Delta_{47\ \mathrm{I\text{-}CDES}}$ values for ETH-2 on Nu Perspective-1, Nu Perspective-2, and MAT 253. **C)** $\Delta_{47\ \mathrm{I\text{-}CDES}}$ values for ETH-3 on Nu Perspective-1, Nu Perspective-2, and MAT 253. **D)** $\Delta_{47\ \mathrm{I\text{-}CDES}}$ values for ETH-4 on Nu Perspective-1, Nu Perspective-2, and MAT 253. **E)** $\Delta_{47\ \mathrm{I\text{-}CDES}}$ values for TV03 on Nu Perspective-1, and MAT 253. **F)** $\Delta_{47\ \mathrm{I\text{-}CDES}}$ values for Veinstrom on Nu Perspective-1, Nu Perspective-2, and MAT 253. **G)** $\Delta_{48\ \mathrm{CDES\ 90}}$ values for ETH-1 on Nu Perspective-1, Nu Perspective-2, Nu Perspective-EG and MAT 253. **H)** $\Delta_{48\ \mathrm{CDES\ 90}}$ values for ETH-2 on Nu Perspective-1, Nu Perspective-2, Nu Perspective-EG and MAT 253. **I)** $\Delta_{48\ \mathrm{CDES\ 90}}$ values for ETH-3 on Nu Perspective-1, Nu Perspective-2, Nu Perspective-EG and MAT 253. **J)** $\Delta_{48\ \mathrm{CDES\ 90}}$ values for ETH-4 on Nu Perspective-1, Nu Perspective-2, Nu Perspective-EG and MAT 253. **K)** $\Delta_{48\ \mathrm{CDES\ 90}}$ values for TV03 on Nu Perspective-1, Nu Perspective-EG and MAT 253. **J)** $\Delta_{48\ \mathrm{CDES\ 90}}$ values for Veinstrom on Nu Perspective-1, Nu Perspective-2, Nu Perspective-EG and MAT 253.

Figure 9. A) Plot showing comparison between anchor standard ETH-1, ETH-2, and ETH-3 $\Delta_{47\ \mathrm{CDES\ 90}}$ values determined on Nu Perspective-EG in this study and Bernasconi et al.[11] **B)** Comparison between consistency standards, IAEA-C1, ETH-4, Merck, and IAEA-C2 from Nu Perspective-1, Nu Perspective-2, and MAT-253 from study and Bernasconi et al.[11] Error bars indicate 1 standard error.

Figure 10. Plot showing comparison between $\Delta_{47\ \mathrm{CDES\ 90}}$ and $\Delta_{48\ \mathrm{CDES\ 90}}$ values for ETH-1, ETH-2, ETH-3, ETH-4, and Carrara Marble from Nu Perspective-EG from this study with values from Fiebig et al.[7], Bajnai et al.[12], and Swart et al.[13] All data in this plot were standardized with 25 ^{o}C and 1000 ^{o}C equilibrated gas-based standardization. Error bars indicate 1 standard error.

Figure 11. A) Plot showing $\Delta_{47\ \mathrm{I\text{-}CDES}}$ and $\Delta_{48\ \mathrm{CDES\ 90}}$ values for 21 carbonate standards, including Devils Hole DH-2 cave calcite. A second order polynomial was fitted through all samples, with the exception of 47407 Coral, which may express kinetic bias. The light blue shading indicates the 95 % confidence interval. Also shown is a temperature-dependent equilibrium regression calculated using theoretical calcite equilibrium Δ_{63} and Δ_{64}[4,5] combined with experimental AFFs

to determine $\Delta_{47\ \text{I-CDES}}$ and $\Delta_{48\ \text{CDES 90}}$ values. Error bars indicate 1 SE. **B)** Experimental Δ_{47} and Δ_{48} data from this study, Swart et al.[13], and Fiebig et al.[14] The data from this study are the same as for panel A, with the exception of 47407 Coral. The data from Fiebig et al.[14] includes lake and cave calcites, inorganic precipitations, and samples equilibrated at high temperatures, with samples having crystallization temperatures of 8 ^{o}C to 1100 ^{o}C. Sample data from Swart et al.[13] include inorganic precipitation from 5 ^{o}C to 65 ^{o}C, and ETH-1, ETH-2, ETH-3, and ETH-4. The individual regressions fit through each dataset were determined to be statistically indistinguishable ($F = 0.43$; $p = 0.86$), and a combined data regression was determined including all three datasets. The grey shading indicates the 95 % confidence interval.

Figure 12. Plot showing Δ_{47} and $\Delta_{48\ \text{CDES 90}}$ values for Devils Hole cave calcite determined in this study, Bajnai et al.[33] and Fiebig et al.[14] The open points indicate individual samples, and solid points are the overall average from each study. See Table 6 for detailed information about sample age, core, and standardization method.

Figure 13. Constraints on acid digestion fractionation factors. **A)** Regression for the acid digestion fractionation factor, $\Delta^*_{63\text{-}47}$, vs theoretical Δ_{63}[4,5]. **B)** Regression for the acid digestion fractionation factor, $\Delta^*_{64\text{-}48}$ vs theoretical Δ_{64}[4,5]. **C)** Regression for acid digestion fractionation factor, $\Delta^*_{63\text{-}47}$, vs precipitation temperature (^{o}C), where $r^2 = 0.9999$. **D)** Regression for the acid digestion fractionation factor, $\Delta^*_{64\text{-}48}$ vs precipitation temperature from 0-300 ^{o}C, where $r^2 = 1$. **E)** Regression for the acid digestion fractionation factor, $\Delta^*_{64\text{-}48}$ vs precipitation temperature from 300-1000 ^{o}C, where $r^2 = 0.9998$. **F)** Regression for acid digestion fractionation factors, $\Delta^*_{64\text{-}48}$ vs $\Delta^*_{63\text{-}47}$, where $r^2 = 1$. Numbers on regression indicate temperature in Celsius.

Figure 14. Relationships for use in determining unknown sample acid digestion fractionation factors, $\Delta^*_{63\text{-}47}$and $\Delta^*_{64\text{-}48}$, and calcite mineral clumped isotope values, Δ_{63} and Δ_{64}. **A)** Regression for acid digestion fractionation factor $\Delta^*_{63\text{-}47}$ vs $\Delta_{47\ \text{I-CDES}}$. **B)** Regression for acid digestion fractionation factor $\Delta^*_{64\text{-}48}$ vs $\Delta_{48\ \text{CDES 90}}$. **C)** Regression for theoretical Δ_{63} vs $\Delta_{47\ \text{I-CDES}}$, where $r^2 = 1$. **D)** Regression for theoretical Δ_{64} vs $\Delta_{48\ \text{CDES 90}}$ vs, where $r^2 = 1$. Numbers on regressions indicate temperature in Celsius.

Figure 15. Comparison of possible equilibrium relationships for Δ_{47} and Δ_{48} values from this study, Fiebig et al.[14], Swart et al.[13], and Bajnai et al.[12] For the temperature range **A)** 0-40 ^{o}C, there are eight regressions shown. The gray line is for the regression fit through the combined experimental datasets from this study, Fiebig et al.[14] and Swart et al.[13], which were determined to produce statistically indistinguishable individual regressions ($F = 0.43$; $p = 0.86$), with the gray shading indicating the 95 % confidence interval. The blue line is the experimental regression from this study fit through 20 carbonates, including Devils Hole calcite, with the blue shading indicating the 95 % confidence interval. The pink circles, purple squares, and green triangles are temperature-dependent equilibrium regressions determined here using a combination of theory

from Hill et al.[4] and Tripati et al.[5] for calcite mineral Δ_{63} and Δ_{64} with experimentally determined AFFs relying on a regression-form AFF, a constant AFF determined at 33.7 °C, and a constant AFF determined at 600 °C, respectively. The black stars and orange asterisks indicate the experimentally determined temperature-dependent equilibrium relationships from Fiebig et al.[14] and Swart et al.[13], respectively. The gray diamonds indicate the temperature-dependent equilibrium regression from Bajnai et al.[12] using a combination of theory from Hill et al.[4] for calcite mineral Δ_{63} and Δ_{64} with experimentally determined AFFs. For the temperature range **B)** 100-600 °C, the regressions are the same as in panel A, with the exception that the regression from Bajnai et al.[12] is not shown due to their regression being calculated for 0-40 °C. Numbers on regressions indicate temperature in Celsius. Overall, it was determined that theoretically based regressions using a regression-form AFF are the most representative of experimental data.

Table 1. Description of the mineralogy and origin for 22 carbonates analyzed in this study (Upadhyay et al., 2021; Chang et al., 2020; Bernasconi et al., 2018), including 4 samples of Devils Hole calcite measured in Tripati et al. (2015). Uranium-series ages for Devils Hole vein calcite were determined by Winograd et al. (2006).

Standard	Mineralogy	Origin
102-GC-AZ01	calcite	Vein carbonate from Grand Canyon
Carmel Chalk	calcite	Chalk
Carrara Marble	calcite	Collected in Carrara, Tuscany, Italy.
CM Tile	calcite	Homogenized version of Carrara Marble (UCLA)
47407 Coral	aragonite	Deep sea coral, *Desmophyllum*
DH-2-10	calcite	Devils Hole - U.S. Geological Survey, Ash Meadows, Nevada. Core DH-2. 172 ± 4 ka
DH-2-11	calcite	Devils Hole - U.S. Geological Survey, Ash Meadows, Nevada. Core DH-2. 163 ± 5 ka
DH-2-12	calcite	Devils Hole - U.S. Geological Survey, Ash Meadows, Nevada. Core DH-2. 157 ± 5 ka
DH-2-13	calcite	Devils Hole - U.S. Geological Survey, Ash Meadows, Nevada. Core DH-2. 151 ± 4 ka
ETH-1	calcite	Carrara Marble, heated to 600°C at 155 MPa for 10 hours, sent from ETH Zurich
ETH-2	calcite	Reagent grade synthetic, subjected to same treatment as ETH-1, sent from ETH Zurich
ETH-3	calcite	Upper Cretaceous chalk (mostly coccoliths), Isle of Rügen, Germany, sent from ETH Zurich
ETH-4	calcite	Same reagent grade synthetic as ETH-2, but unheated, sent from ETH Zurich
IAEA-C1	calcite	Carrara Marble, from International Atomic Energy Agency
IAEA-C2	travertine	Collected in Bavaria. From International Atomic Energy Agency
ISTB-1	calcite	Speleothem from Yichang, Hubei province, China
Mallinckrodt	calcite	Synthetic, from Mallinckrodt Baker, Inc.
MERCK	calcite	Synthetic, from International Atomic Energy Agency
NBS 19	calcitic marble	Carrara Marble, from National Bureau of Standards
Spel 2-8-E	calcite	Speleothem
SRM 88B	dolomitic limestone	Collected from mine site near Skokie, Illinois, USA
TB-1	marble	Marble rock of marine origin from Quyang, Hebei province, China
TB-2	calcite	Hydrothermal calcite from Yanji, Jilin province, China
TV01	calcite	Travertine tile
TV03	calcite	Travertine tile
Veinstrom	calcite	Shallow carbonate vein collected from Tempiute Mountain, Nevada

Table 2. Description of mass spectrometer configurations used in this study. Δ_{48} data from the MAT 253 was not used to calculate the combined instrument average.

Configuration	Mass spectrometer model	Acid digestion temperature	Acid digestion system, sample size	m/z 44 ion beam intensity	Integration time	Use of equilibrated gas- based corrections	Use of carbonate-based corrections	Δ_{47} reference frame	Δ_{48} reference frame	Long-term instrument reproducibility Δ_{47} SD	Long-term instrument reproducibility Δ_{47} SE	Long-term instrument reproducibility Δ_{48} SD	Long-term instrument reproducibility Δ_{48} SE
Nu Perspective- EG	Nu Instruments Perspective	90 °C	Common acid bath, 0.45-0.60 mg	80 nA before 6/2017, 60 nA after 6/2017	1600 s	Yes, 25 and 1000 °C equilibrated gases	No	CDES 90	CDES 90	0.025	0.004	0.073	0.010
Nu Perspective-1	Nu Instruments Perspective	90 °C	Common acid bath,0.45-0.60 mg	80 nA before 6/2017, 60 nA after 6/2017	1600 s	No	Yes	I-CDES	CDES 90	0.022	0.003	0.052	0.006
Nu Perspective -1a	Nu Instruments Perspective	90 °C	Common acid bath, 0.45-0.60 mg	80-30 nA	1200 s	No	Yes	I-CDES	CDES 90	n/a	n/a	n/a	n/a
Nu Perspective-2	Nu Instruments Perspective	70 °C	NuCarb, 0.45-0.60 mg	80-30 nA	1200 s	No	Yes	I-CDES	CDES 90	0.029	0.004	0.06	0.005
MAT 253	Thermo Finnigan MAT 253	90 °C	Common acid bath, 5-7 mg	16 V	720 s	No	Yes	I-CDES	N/A	0.023	0.005	0.105	0.019

Table 3. $\Delta_{47\ \text{I-CDES}}$ and $\Delta_{48\ \text{CDES 90}}$ estimated marginal means by configuration, with pairwise contrasts adjusted for multiple comparisons. Estimated marginal means are preferred to ordinary marginal means because they control for differences in the number of analyses run on individual configurations. Confidence levels are 95%. We find no evidence of statistically significant differences in the values produced by individual configurations, after controlling for multiple comparisons.

$\Delta_{47\ \text{I-CDES}}$	Mass Spectrometer	Estimated marginal mean	SE	df	Lower CL	Upper CL
	Nu Perspective-1	0.4494	0.0022	16	0.4429	0.456
	Nu Perspective-2	0.447	0.0018	16	0.4416	0.4523
	MAT 253	0.4471	0.0016	16	0.4423	0.4518

Contrast	Difference	SE	df	Lower CL	Upper CL	t ratio	p-value
Nu Perspective-1 - Nu Perspective-2	0.0025	0.0024	16	-0.0048	0.0097	1.03	0.57
Nu Perspective-1 - MAT 253	0.0024	0.0023	16	-0.0046	0.0094	1.033	0.57
Nu Perspective-2 - MAT 253	-0.0001	0.0021	16	-0.0064	0.0062	-0.05	0.999

$\Delta_{48\ \text{CDES 90}}$	Mass Spectrometer	Estimated marginal mean	SE	df	Lower CL	Upper CL
	Nu Perspective-EG	0.2139	0.0055	25	0.1971	0.2308
	Nu Perspective-1	0.2084	0.0057	25	0.1908	0.2261
	Nu Perspective-2	0.2105	0.0049	25	0.1956	0.2255
	MAT 253	0.2081	0.0045	25	0.1941	0.222

Contrast	Difference	SE	df	Lower CL	Upper CL	t ratio	p-value
Nu Perspective-EG - Nu Perspective-1	0.0055	0.0069	25	-0.0156	0.0267	0.804	0.8518
Nu Perspective-EG - Nu Perspective-2	0.0034	0.0066	25	-0.0169	0.0237	0.515	0.9547
Nu Perspective-EG - MAT 253	0.0059	0.0065	25	-0.0142	0.026	0.904	0.8028
Nu Perspective-1 - Nu Perspective-2	-0.0021	0.0061	25	-0.0209	0.0167	-0.35	0.9853
Nu Perspective-1 - MAT 253	0.0004	0.006	25	-0.0182	0.019	0.062	0.9999
Nu Perspective-2 - MAT 253	0.0025	0.0053	25	-0.014	0.019	0.467	0.9656

Table 4. Differences in final mean, standard deviation, and N for $\Delta_{47\ \text{I-CDES}}$ and $\Delta_{48\ \text{CDES-90}}$ from different instruments when employing cutoffs at 3σ and 5σ for the anchor standards ETH-1 and ETH-2, and the consistency standards ETH-4 and Veinstrom.

			3σ cutoff			5σ cutoff			Absolute difference		
Mass Spec	**Standard**	**Raw N**	**Final mean**	**Final SD**	**Final N**	**Final mean**	**Final SD**	**Final N**	**Mean**	**SD**	**N**
Nu Perspective-1 $\Delta_{47\ \text{I-CDES}}$	ETH-1	91	0.2066	0.025	85	0.2076	0.026	86	0.001	0.0014	1
	ETH-2	76	0.2081	0.020	69	0.2081	0.020	69	0	0	0
	ETH-4	74	0.4552	0.020	64	0.4552	0.020	64	0	0	0
	Veinstrom	107	0.6365	0.026	102	0.6365	0.026	102	0	0	0
Nu Perspective-2 $\Delta_{47\ \text{I-CDES}}$	ETH-1	425	0.2053	0.026	402	0.2055	0.026	403	0.0002	0.0003	1
	ETH-2	393	0.2060	0.027	386	0.2065	0.028	390	0.0005	0.0016	4
	ETH-4	194	0.4411	0.026	191	0.4420	0.027	193	0.0009	0.0015	2
	Veinstrom	345	0.6341	0.030	322	0.6338	0.030	323	0.0003	0.0004	1
MAT 253 $\Delta_{47\ \text{I-CDES}}$	ETH-1	292	0.2063	0.020	284	0.2063	0.020	284	0	0	0
	ETH-2	275	0.2066	0.024	271	0.2063	0.024	272	0.0003	0.0005	1
	ETH-4	215	0.4451	0.021	208	0.4448	0.021	209	0.0003	0.0005	1
	Veinstrom	308	0.6315	0.023	304	0.6318	0.023	305	0.0003	0.0004	1
Nu Perspective-1 $\Delta_{48\ \text{CDES 90}}$	ETH-1	91	0.1301	0.051	88	0.1301	0.051	88	0	0	0
	ETH-2	80	0.1309	0.064	73	0.1309	0.064	73	0	0	0
	ETH-4	75	0.1975	0.059	70	0.1975	0.059	70	0	0	0
	Veinstrom	103	0.2722	0.066	100	0.2722	0.066	100	0	0	0
Nu Perspective-2 $\Delta_{48\ \text{CDES 90}}$	ETH-1	389	0.1327	0.065	376	0.1327	0.067	378	0	0.0018	2
	ETH-2	381	0.1326	0.056	366	0.1321	0.057	367	0.0005	0.0007	1
	ETH-4	190	0.2028	0.058	187	0.2028	0.058	187	0	0	0
	Veinstrom	358	0.2739	0.059	336	0.2739	0.059	336	0	0	0

Table 5. $\Delta_{48\ CDES\ 90}$ for carbonates analyzed on Nu Perspective-EG. All data in this table was standardized using only 25 and 1000 ^{o}C equilibrated gases. Results are compared to values from Fiebig et al., (2019), Bajnai et al. (2020), and Swart et al. (2021).

Standard	This study, Nu Perspective-EG						Bernasconi et al., 2021			Fiebig et al., 2019					Fiebig et al., 2019; Bajnai et al., 2020					Swart et al., 2021				
	N	$\Delta_{47\ CDES\ 90}$ (‰)	Δ_{47} SE	N	$\Delta_{48\ CDES\ 90}$ (‰)	Δ_{48} SE	N	$\Delta_{47\ CDES\ 90}$ (‰)	Δ_{47} SE	N	$\Delta_{47\ CDES\ 90}$ (‰)	Δ_{47} SE	$\Delta_{48\ CDES\ 90}$ (‰)	Δ_{48} SE	N	$\Delta_{47\ CDES\ 90}$ (‰)	Δ_{47} SE	$\Delta_{48\ CDES\ 90}$ (‰)	Δ_{48} SE	N	$\Delta_{47\ CDES\ 90}$ (‰)	Δ_{47} SE	$\Delta_{48\ CDES\ 90}$ (‰)	Δ_{48} 95% confidence interval
Carrara Marble	62	0.318	0.004	64	0.160	0.010				12	0.314	0.003	0.140	0.012										
ETH-1	36	0.205	0.004	44	0.133	0.011	232	0.205	0.002						78	0.212	0.001	0.142	0.004	19	0.214	0.006	0.145	0.012
ETH-2	30	0.200	0.004	36	0.130	0.013	215	0.208	0.001						71	0.212	0.002	0.138	0.004	14	0.203	0.004	0.153	0.011
ETH-3	35	0.617	0.003	45	0.261	0.009	264	0.613	0.001						74	0.615	0.001	0.299	0.005	20	0.629	0.005	0.269	0.007
ETH-4	36	0.462	0.004	45	0.201	0.014	162	0.450	0.002	11	0.457	0.003	0.223	0.010						14	0.459	0.005	0.231	0.010
TV03	56	0.637	0.005	55	0.269	0.007																		
Veinstrom	69	0.643	0.004	74	0.263	0.010																		

Table 6. Individual instrument and longterm combined average $\Delta_{47\ I\text{-}CDES}$ and $\Delta_{48\ CDES\ 90}$ for all carbonates analyzed in this study. $\Delta_{48\ CDES\ 90}$ values from MAT 253 (gray columns) were not used in the combined instrument average.

	Combined average				Combined average				Nu Perspective 1								Nu Perspective 2								MAT 253							
Standard	$\Delta_{47\ I\text{-}CDES}$ (‰)	N	Δ_{47} SD	Δ_{47} SE	$\Delta_{48\ CDES\ 90}$ (‰)	N	Δ_{48} SD	Δ_{48} SE	$\Delta_{47\ I\text{-}CDES}$ (‰)	N	Δ_{47} SD	Δ_{47} SE	$\Delta_{48\ CDES\ 90}$ (‰)	N	Δ_{48} SD	Δ_{48} SE	$\Delta_{47\ I\text{-}CDES}$ (‰)	N	Δ_{47} SD	Δ_{47} SE	$\Delta_{48\ CDES\ 90}$ (‰)	N	Δ_{48} SD	Δ_{48} SE	$\Delta_{47\ I\text{-}CDES}$ (‰)	N	Δ_{47} SD	Δ_{47} SE	*$\Delta_{48\ CDES\ 90}$ (‰)*	*N*	*Δ_{48} SD*	*Δ_{48} SE*
102-GC-AZ01	0.598	24	0.028	0.006	0.240	24	0.057	0.012																								
Carmel Chalk	0.592	640	0.025	0.001	0.237	319	0.056	0.003	0.591	94	0.017	0.002	0.243	69	0.028	0.003	0.589	248	0.026	0.002	0.235	250	0.062	0.004	0.594	282	0.021	0.001	*0.227*	*166*	*0.080*	*0.006*
Carrara Marble	0.314	280	0.030	0.002	0.151	135	0.079	0.006	0.312	81	0.031	0.003	0.146	81	0.072	0.008	0.328	44	0.048	0.007	0.159	54	0.065	0.009	0.310	155	0.020	0.002	*0.175*	*80*	*0.161*	*0.018*
Carrara Marble CIT	0.326	21	0.027	0.006	0.144	24	0.081	0.017																								
CMTile	0.313	463	0.026	0.001	0.145	309	0.059	0.003					0.149	18	0.029	0.007	0.315	303	0.029	0.002	0.145	291	0.060	0.004	0.310	160	0.019	0.001	*0.156*	*144*	*0.098*	*0.008*
47407 Coral	0.707	9	0.025	0.008	0.275	11	0.071	0.021																								
DH-2-10	0.554	11	0.013	0.004	0.236	16	0.082	0.020																								
DH-2-11	0.560	19	0.027	0.006	0.196	17	0.035	0.009																								
DH-2-12	0.564	18	0.025	0.006	0.243	16	0.032	0.008																								
DH-2-13	0.568	17	0.027	0.006	0.261	19	0.063	0.014																								
DH-2 Combined	0.566	74	0.028	0.003	0.240	76	0.068	0.008																								
ETH-1	0.206	771	0.023	0.001	0.132	464	0.062	0.003	0.207	85	0.025	0.003	0.130	88	0.051	0.005	0.205	402	0.026	0.001	0.133	376	0.065	0.003	0.206	284	0.020	0.001	*0.139*	*188*	*0.105*	*0.008*
ETH-2	0.206	726	0.025	0.001	0.132	439	0.058	0.003	0.208	69	0.020	0.002	0.131	73	0.064	0.008	0.206	386	0.027	0.001	0.133	366	0.056	0.003	0.207	271	0.024	0.001	*0.156*	*204*	*0.110*	*0.008*
ETH-3	0.609	463	0.025	0.001	0.247	236	0.057	0.004	0.612	69	0.023	0.003	0.244	68	0.054	0.007	0.602	184	0.027	0.002	0.249	168	0.058	0.004	0.614	210	0.022	0.002	*0.250*	*145*	*0.082*	*0.007*
ETH-4	0.445	463	0.023	0.001	0.201	257	0.058	0.004	0.455	64	0.020	0.003	0.198	70	0.059	0.007	0.441	191	0.026	0.002	0.203	187	0.058	0.004	0.445	208	0.021	0.001	*0.206*	*171*	*0.106*	*0.008*
IAEA-C1	0.299	83	0.024	0.003	0.143	49	0.056	0.008									0.300	68	0.025	0.003	0.143	49	0.056	0.008	0.294	15	0.017	0.004	*0.142*	*15*	*0.141*	*0.036*
IAEA-C2	0.638	74	0.025	0.003	0.273	59	0.062	0.008									0.642	60	0.025	0.003	0.273	59	0.062	0.008	0.624	14	0.021	0.005	*0.236*	*13*	*0.067*	*0.018*
ISTB-1	0.663	15	0.059	0.015	0.297	12	0.047	0.014																								
Mallinckrodt	0.465	16	0.042	0.011																					0.465	16	0.042	0.011	*0.136*	*13*	*0.081*	*0.023*
Merck	0.514	81	0.030	0.003	0.234	59	0.055	0.007									0.514	67	0.030	0.004	0.234	59	0.055	0.007	0.514	14	0.030	0.008	*0.175*	*11*	*0.170*	*0.051*
NBS 19	0.316	8	0.025	0.009																					0.316	8	0.025	0.009	*0.116*	*7*	*0.073*	*0.027*
SPEL-2-8-E	0.596	11	0.035	0.011	0.245	11	0.089	0.027																								
SRM88B	0.528	11	0.017	0.005																					0.528	11	0.017	0.005	*0.424*	*10*	*0.153*	*0.048*
TB-1	0.327	21	0.034	0.007	0.133	23	0.089	0.019																								
TB-2	0.335	19	0.035	0.008	0.164	19	0.095	0.022																								
TV01	0.619	22	0.028	0.006	0.260	25	0.077	0.015																								
TV03	0.626	127	0.019	0.002	0.267	58	0.043	0.006	0.626	47	0.019	0.003	0.267	58	0.043	0.006									0.626	80	0.019	0.002	*0.212*	*32*	*0.063*	*0.011*
Veinstrom	0.633	728	0.026	0.001	0.273	436	0.061	0.003	0.636	102	0.026	0.003	0.272	100	0.066	0.007	0.634	322	0.030	0.002	0.274	336	0.059	0.003	0.632	304	0.023	0.001	*0.252*	*193*	*0.079*	*0.006*

Table 7. Δ_{47} and Δ_{48} data for Devils Hole cave calcite from this study, Bajnai et al. (2021), and Fiebig et al. (2021).

	Sample	Age (ka)	N	$\Delta_{47\ I\text{-}CDES}$ (‰) (carbonate standard corrected using I-CDES values)	$\Delta_{47\ CDES\ 90}$ (‰) (carbonate standard corrected)	Δ_{47} SE	N	$\Delta_{48\ CDES\ 90}$ (‰) (carbonate standard corrected)	Δ_{48} SE	$\Delta_{48\ CDES\ 90}$ (‰) (gas corrected)	Δ_{48} SE
This study	DH-2-10	168-176	11	0.554		0.004	16	0.236	0.020		
	DH-2-11	159-167	19	0.560		0.006	17	0.196	0.009		
	DH-2-12	152-162	18	0.564		0.006	16	0.243	0.008		
	DH-2-13	146-156	17	0.568		0.006	19	0.261	0.014		
	Average		74	0.566		0.003	76	0.240	0.008		
Bajnai et al., 2021	DHC2-8	4.5-16.9	14		0.573	0.002	N is the same as for Δ_{47}	0.255	0.010	0.237	0.007
	DHC2-3	32.2-39.8	9		0.575	0.003		0.252	0.008	0.227	0.008
	DH-11 19.7	86.4-94.3	9		0.572	0.001		0.255	0.009	0.229	0.009
	DH-11 44.5	121.8-123.7	12		0.581	0.002		0.226	0.008	0.210	0.008
	DH-11 73.0	176.1-184.8	9		0.575	0.002		0.250	0.008	0.225	0.008
	DH-11 109.4	232.8-240.5	23		0.575	0.001		0.227	0.005	0.208	0.005
	DH-11 141.6	291.3-299.0	9		0.570	0.002		0.233	0.010	0.208	0.009
	DH-11 189.9	353.0-358.3	14		0.574	0.002		0.232	0.006	0.217	0.007
	DH-11 201.3	371.7-388.4	9		0.568	0.003		0.250	0.010	0.226	0.010
	DH-11 296.6	485.5-507.8	8		0.575	0.002		0.243	0.010	0.222	0.009
	Average		116		0.574	0.003		0.239	0.003	0.221	0.007
Fiebig et al., 2021	DVH-2	4.5-16.9	9	0.582	0.569	0.003	N is the same as for Δ_{47}			0.246	0.012
	DHC2-8	4.5-16.9	8	0.585	0.573	0.003				0.234	0.013
	DHC2-8	4.5-16.9	9	0.572	0.568	0.003				0.234	0.012
	DHC2-8	4.5-16.9	5	0.576	0.568	0.004				0.247	0.016
	Average		22	0.578	0.570	0.002				0.237	0.008

Table 8. Theoretical model equilibrium Δ_{63} and Δ_{64} for calcite (Hill et al., 2014; Tripati et al., 2015), acid digestion fractionation factors $\Delta^*_{63\text{-}47}$ and $\Delta^*_{64\text{-}48}$ for the phosphoric acid digestion of calcite to CO_2, and equilibrium calcite $\Delta_{47\ \text{I-CDES EQ}}$ and $\Delta_{48\ \text{CDES 90 EQ}}$.

T (°C)	Δ_{63} (Hill et al., 2014; Tripati et al., 2015)	$\Delta^*_{63\text{-}47}$	$\Delta_{47\ \text{I-CDES EQ}}$	Δ_{64} (Hill et al., 2014; Tripati et al., 2015)	$\Delta^*_{64\text{-}48}$	$\Delta_{48\ \text{CDES 90 EQ}}$
0	0.470	0.197	0.667	0.156	0.131	0.287
10	0.438	0.196	0.634	0.140	0.131	0.271
20	0.408	0.196	0.604	0.126	0.131	0.257
22	0.402	0.196	0.598	0.123	0.131	0.254
25	0.394	0.195	0.589	0.120	0.131	0.251
30	0.381	0.195	0.576	0.114	0.131	0.245
33.7 (DH-2)	0.371	0.195	0.566	0.109	0.131	0.240
40	0.355	0.195	0.550	0.103	0.131	0.233
50	0.332	0.194	0.526	0.093	0.131	0.224
60	0.310	0.194	0.504	0.084	0.131	0.215
70	0.290	0.193	0.483	0.076	0.131	0.207
80	0.271	0.193	0.464	0.069	0.131	0.200
90	0.254	0.193	0.446	0.063	0.131	0.194
100	0.238	0.192	0.430	0.058	0.130	0.188
200	0.128	0.190	0.318	0.025	0.130	0.155
300	0.073	0.189	0.262	0.012	0.130	0.142
400	0.044	0.189	0.232	0.006	0.130	0.136
500	0.027	0.188	0.216	0.004	0.130	0.134
600	0.018	0.188	0.206	0.002	0.130	0.132
700	0.012	0.188	0.200	0.002	0.130	0.132
800	0.009	0.188	0.197	0.001	0.130	0.131
900	0.006	0.188	0.194	0.001	0.130	0.131
1000	0.005	0.188	0.192	0.001	0.130	0.131

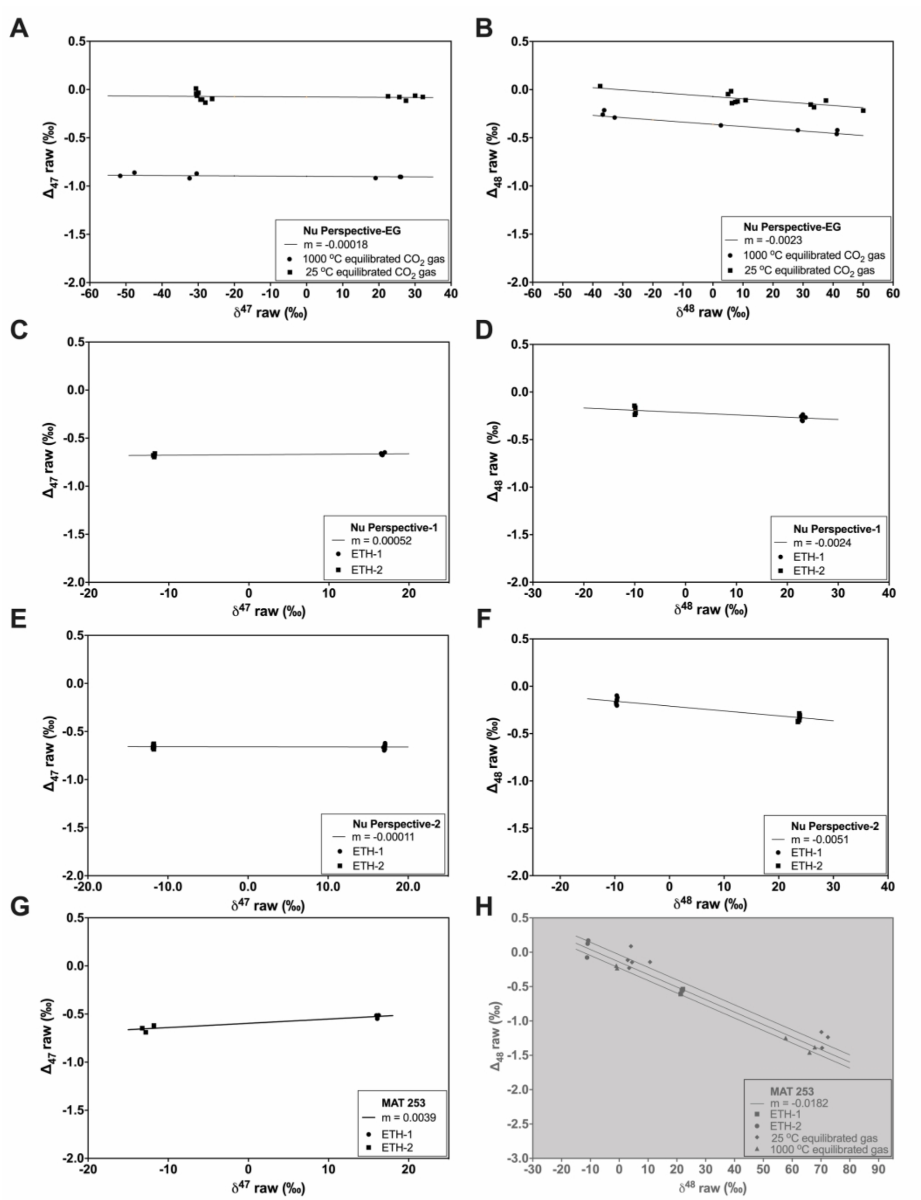

198x255mm (300 x 300 DPI)

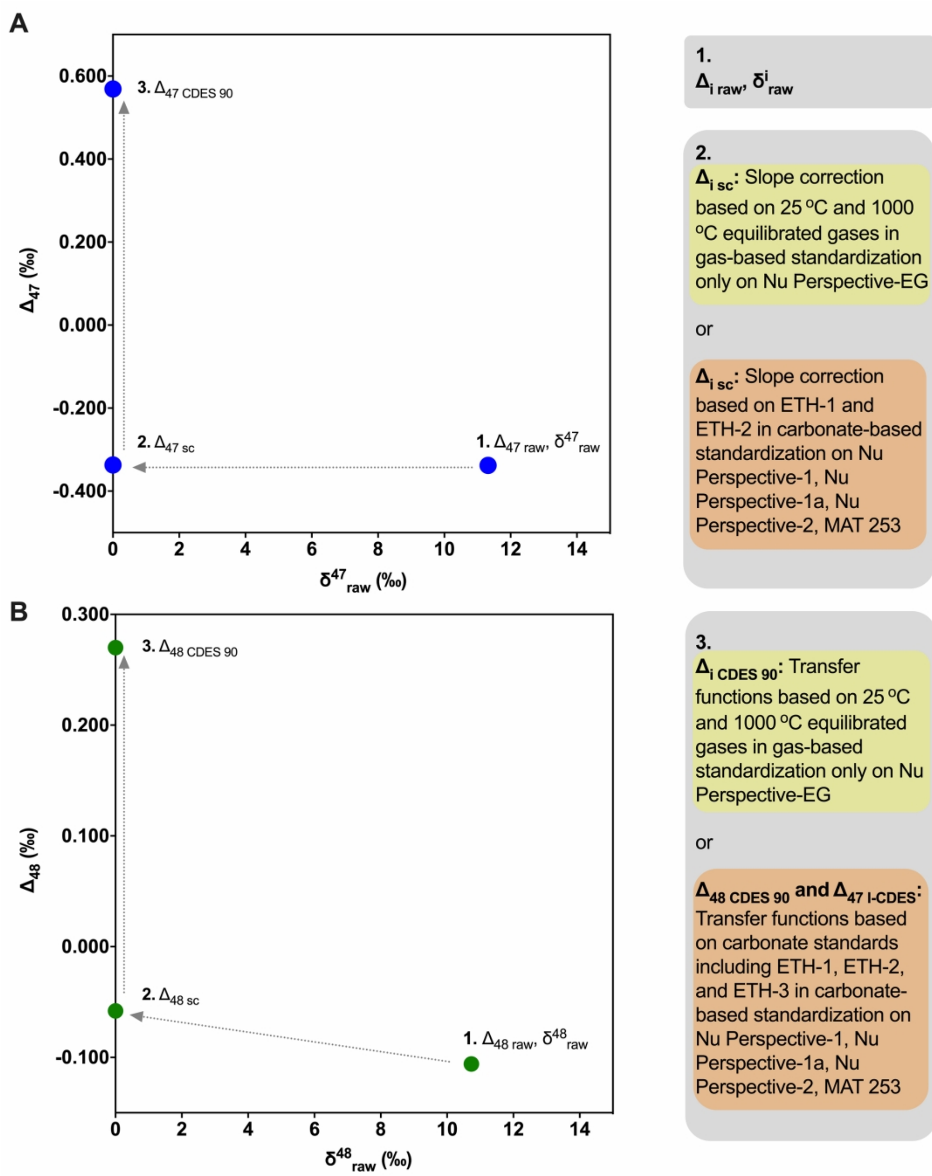

198x253mm (300 x 300 DPI)

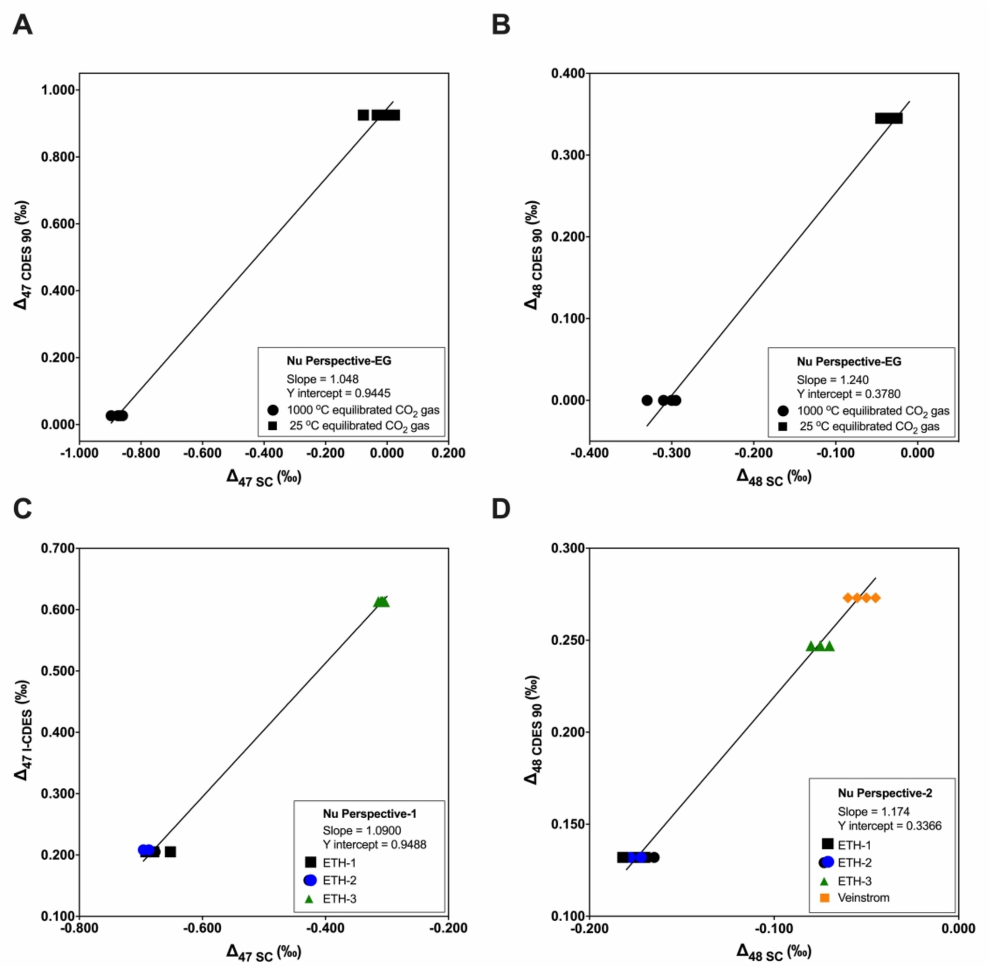

199x194mm (300 x 300 DPI)

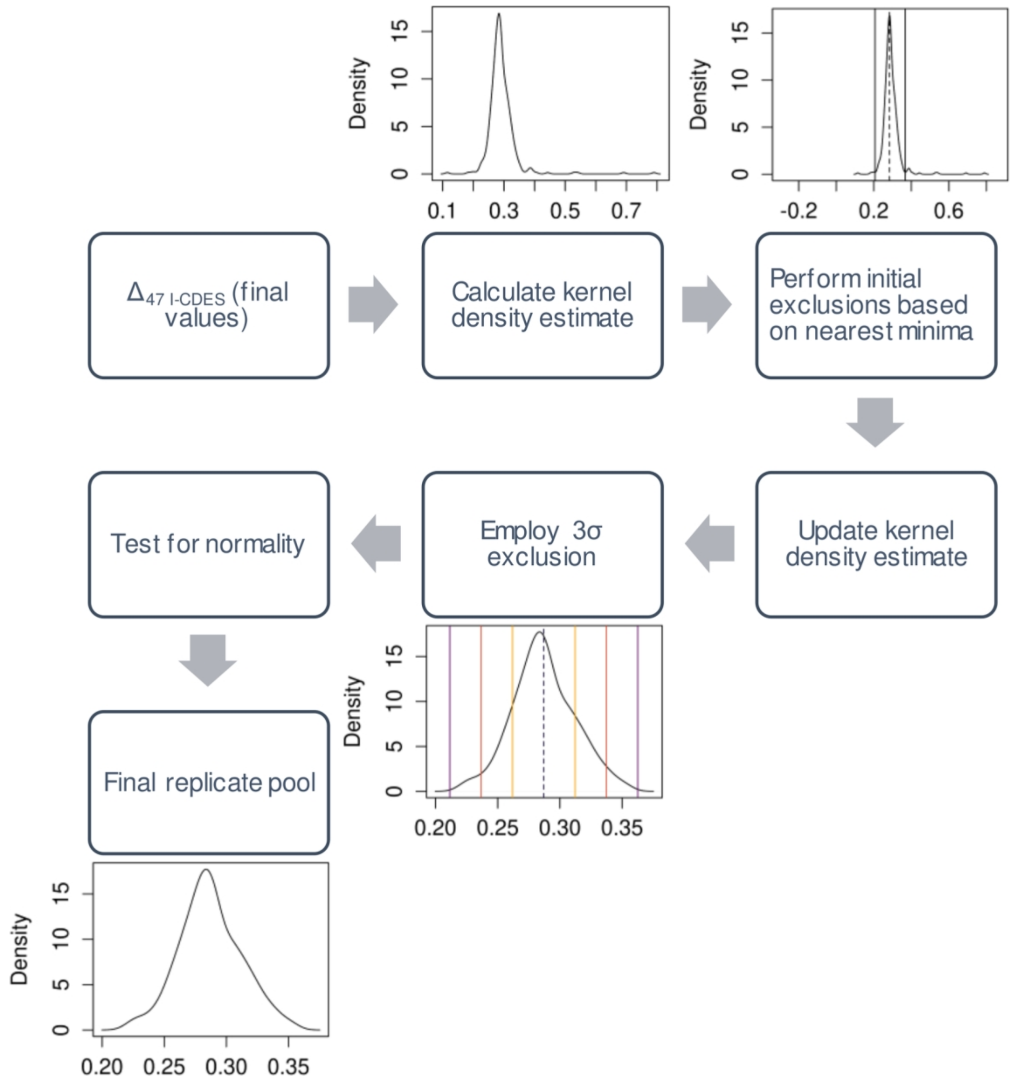

74x79mm (600 x 600 DPI)

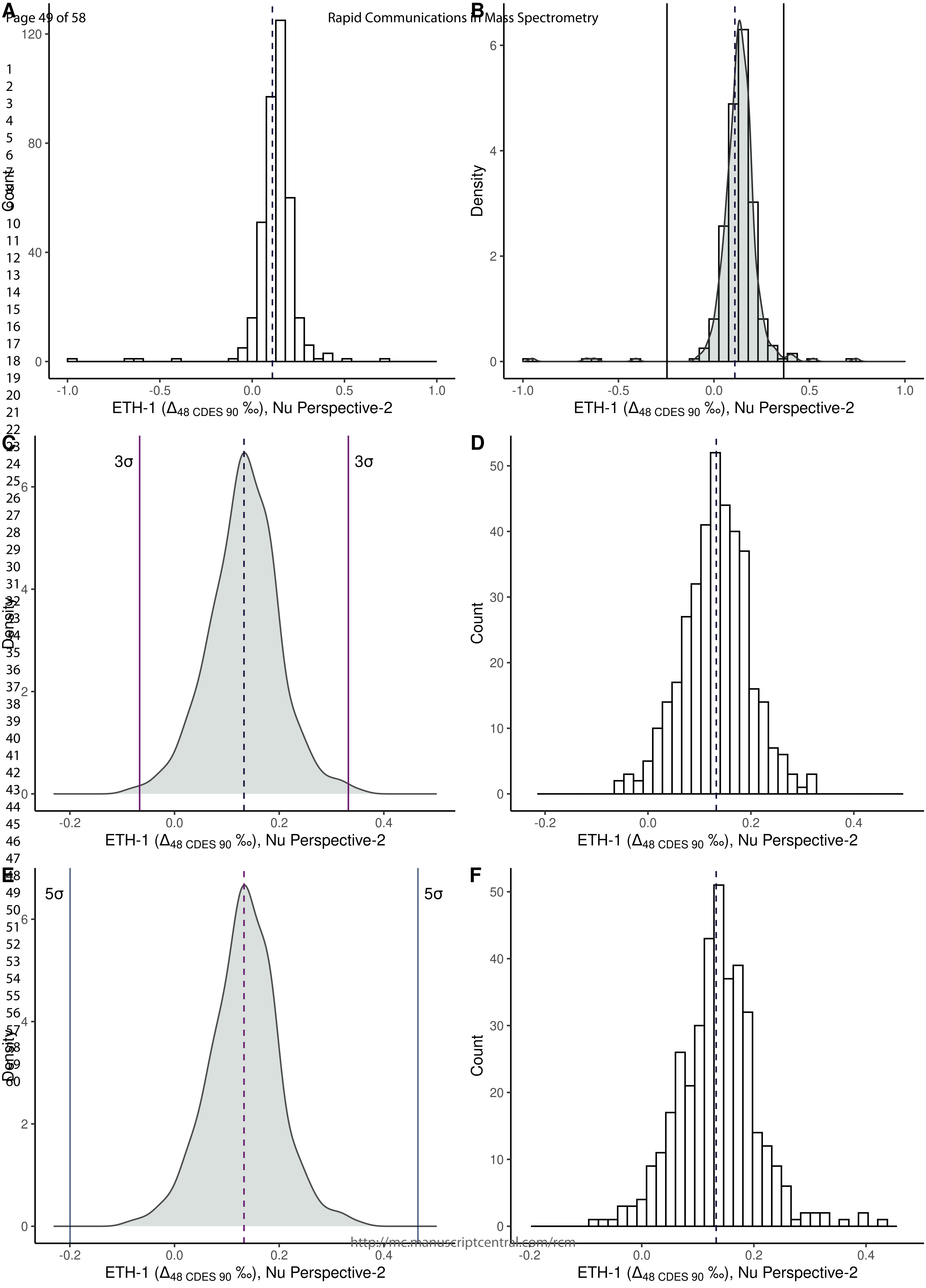
A
B
C
D
E
F
Count
Density
3σ
5σ
ETH-1 ($\Delta_{48\ CDES\ 90}$ ‰), Nu Perspective-2

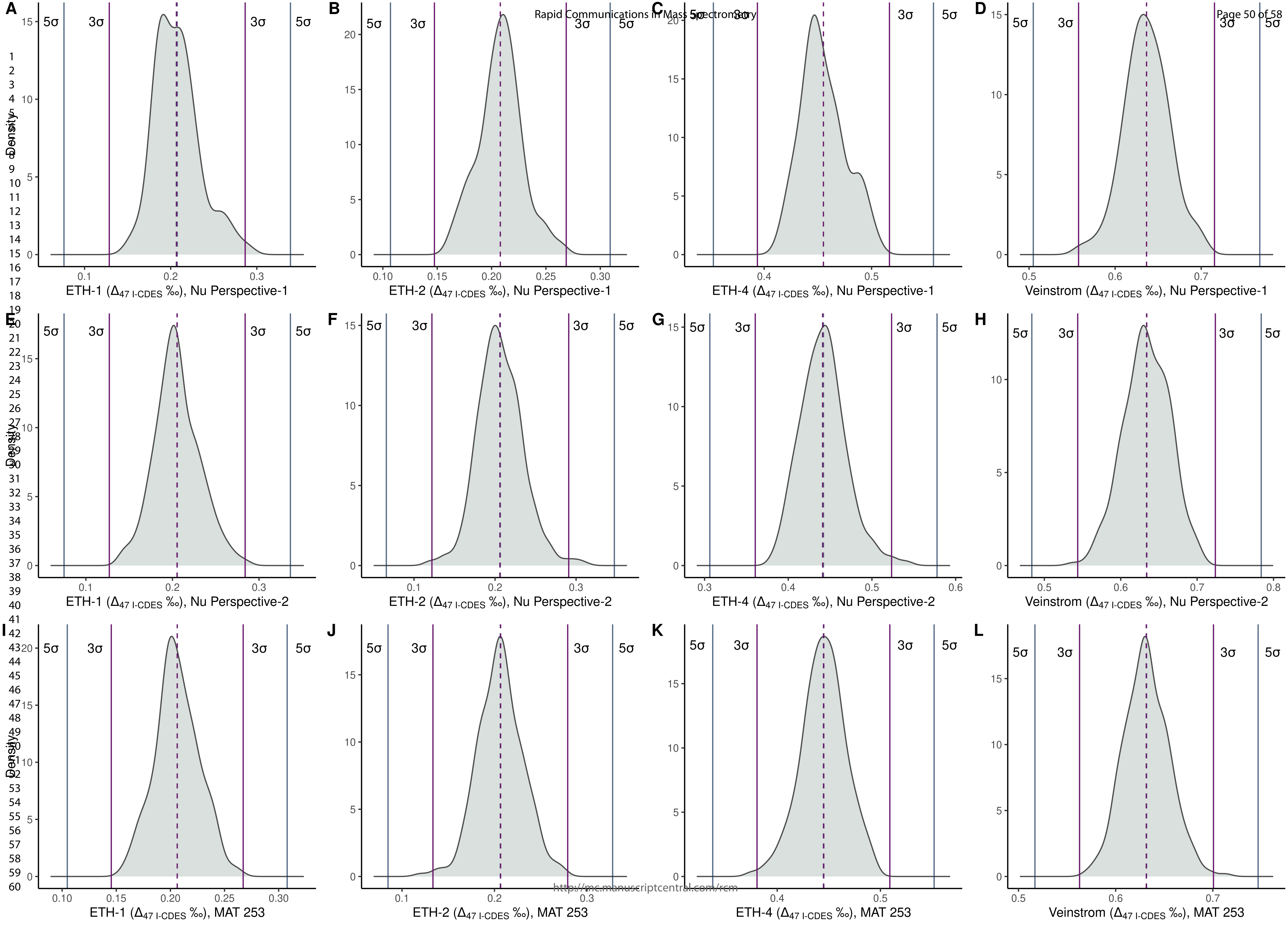
A
B
C
D
E
F
G
H
I
J
K
L
5σ
3σ
Density
ETH-1 ($\Delta_{47\ I\text{-}CDES}$ ‰), Nu Perspective-1
ETH-2 ($\Delta_{47\ I\text{-}CDES}$ ‰), Nu Perspective-1
ETH-4 ($\Delta_{47\ I\text{-}CDES}$ ‰), Nu Perspective-1
Veinstrom ($\Delta_{47\ I\text{-}CDES}$ ‰), Nu Perspective-1
ETH-1 ($\Delta_{47\ I\text{-}CDES}$ ‰), Nu Perspective-2
ETH-2 ($\Delta_{47\ I\text{-}CDES}$ ‰), Nu Perspective-2
ETH-4 ($\Delta_{47\ I\text{-}CDES}$ ‰), Nu Perspective-2
Veinstrom ($\Delta_{47\ I\text{-}CDES}$ ‰), Nu Perspective-2
ETH-1 ($\Delta_{47\ I\text{-}CDES}$ ‰), MAT 253
ETH-2 ($\Delta_{47\ I\text{-}CDES}$ ‰), MAT 253
ETH-4 ($\Delta_{47\ I\text{-}CDES}$ ‰), MAT 253
Veinstrom ($\Delta_{47\ I\text{-}CDES}$ ‰), MAT 253

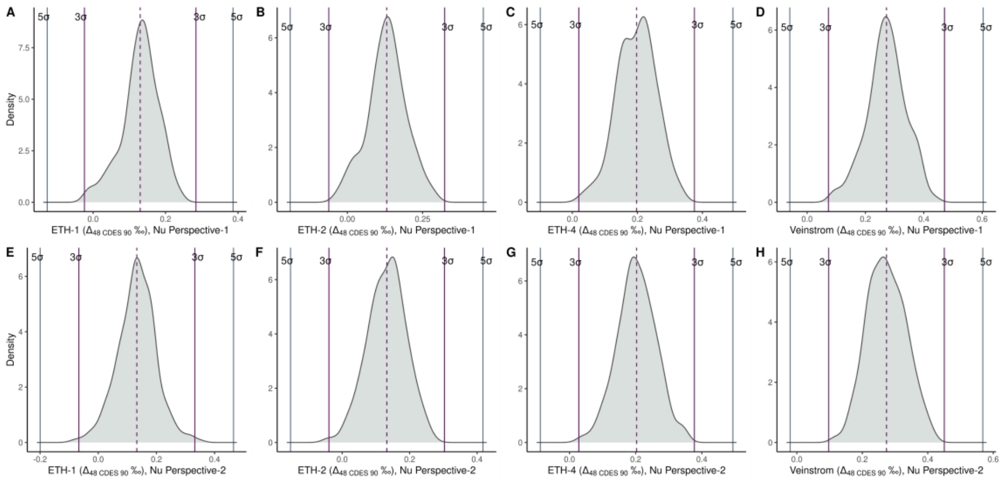

228x109mm (600 x 600 DPI)

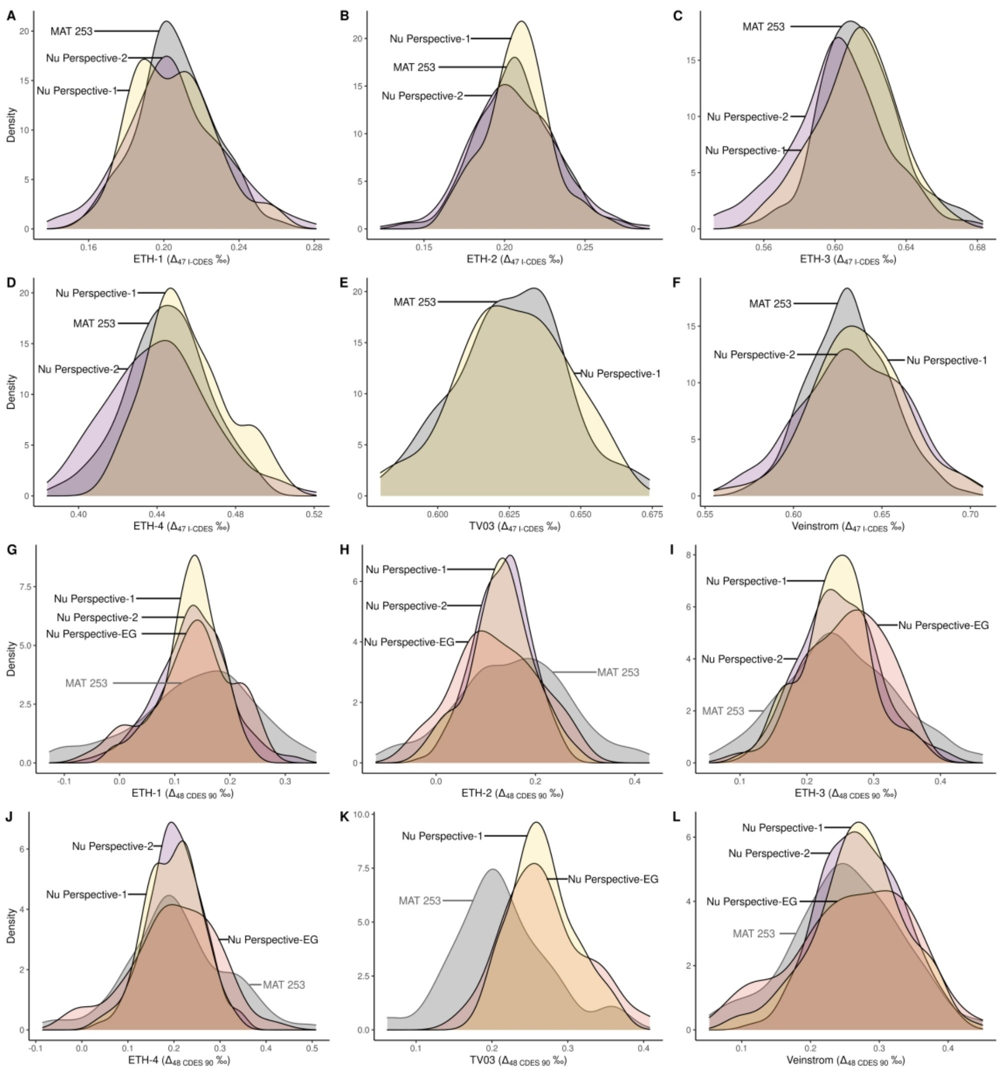

165x176mm (600 x 600 DPI)

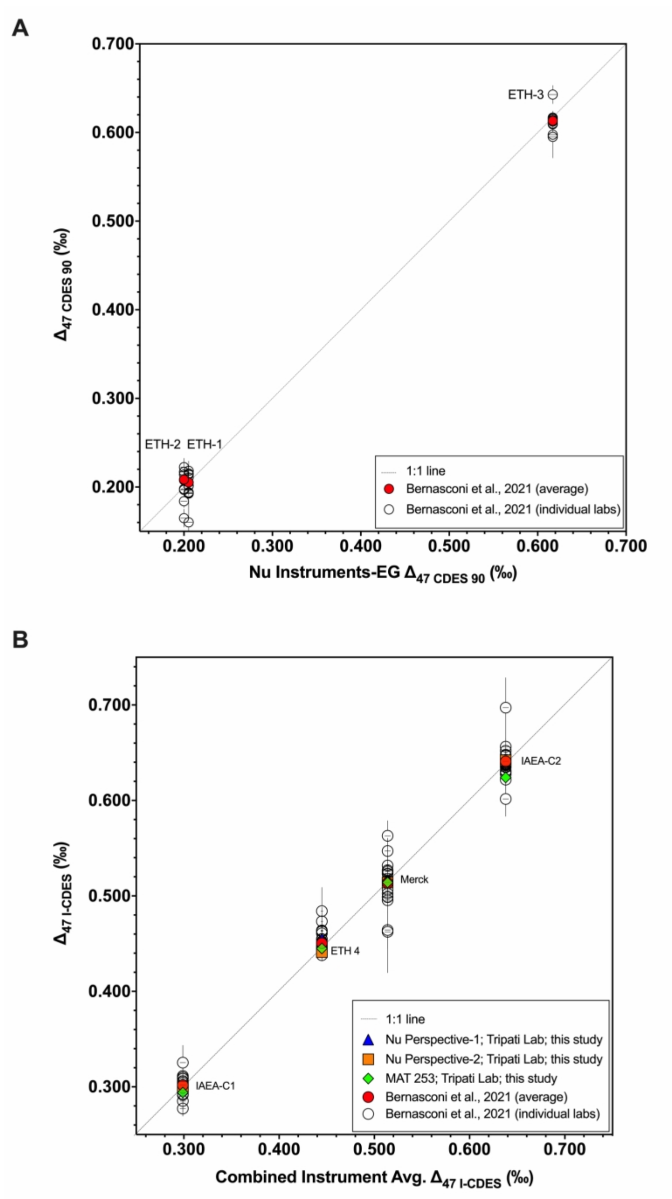

141x250mm (300 x 300 DPI)

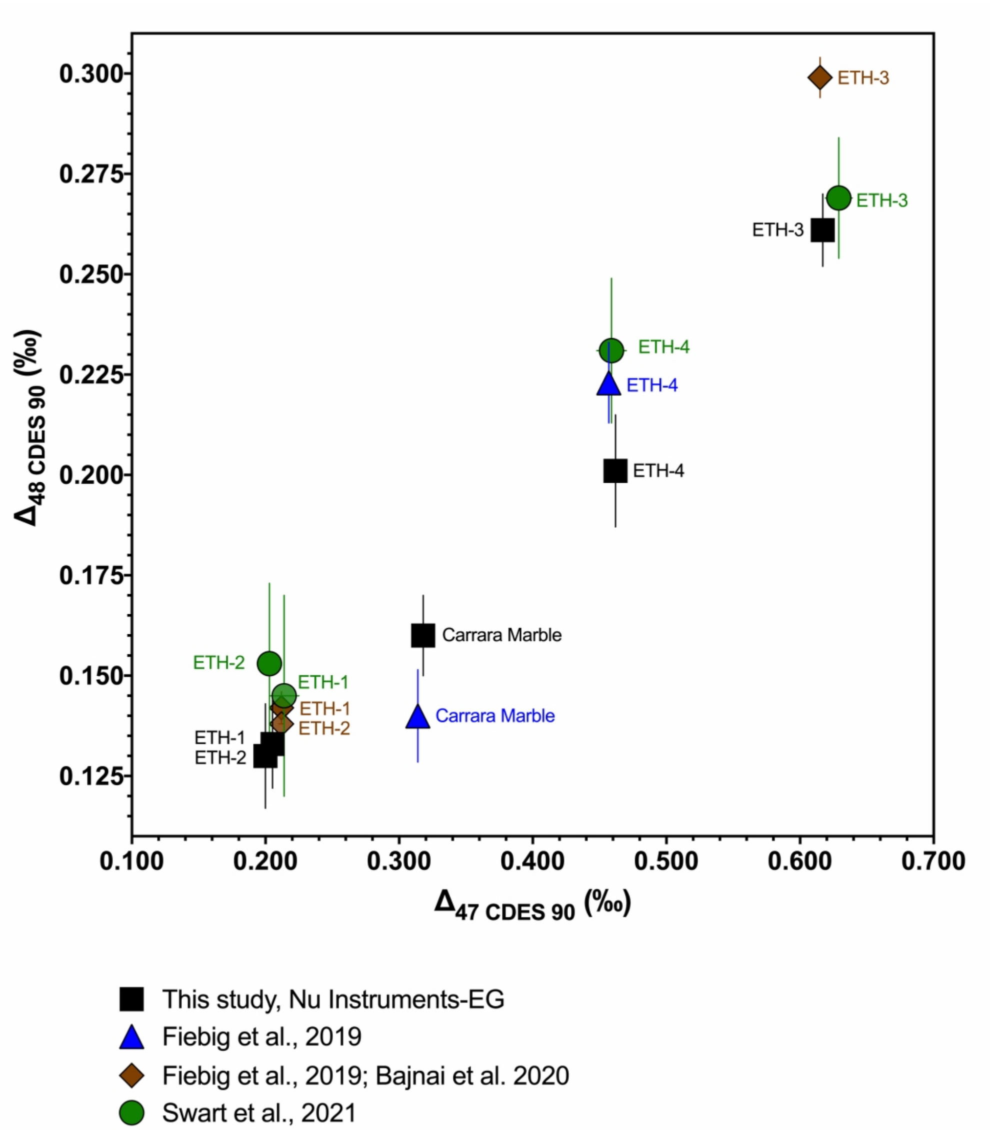

190x215mm (300 x 300 DPI)

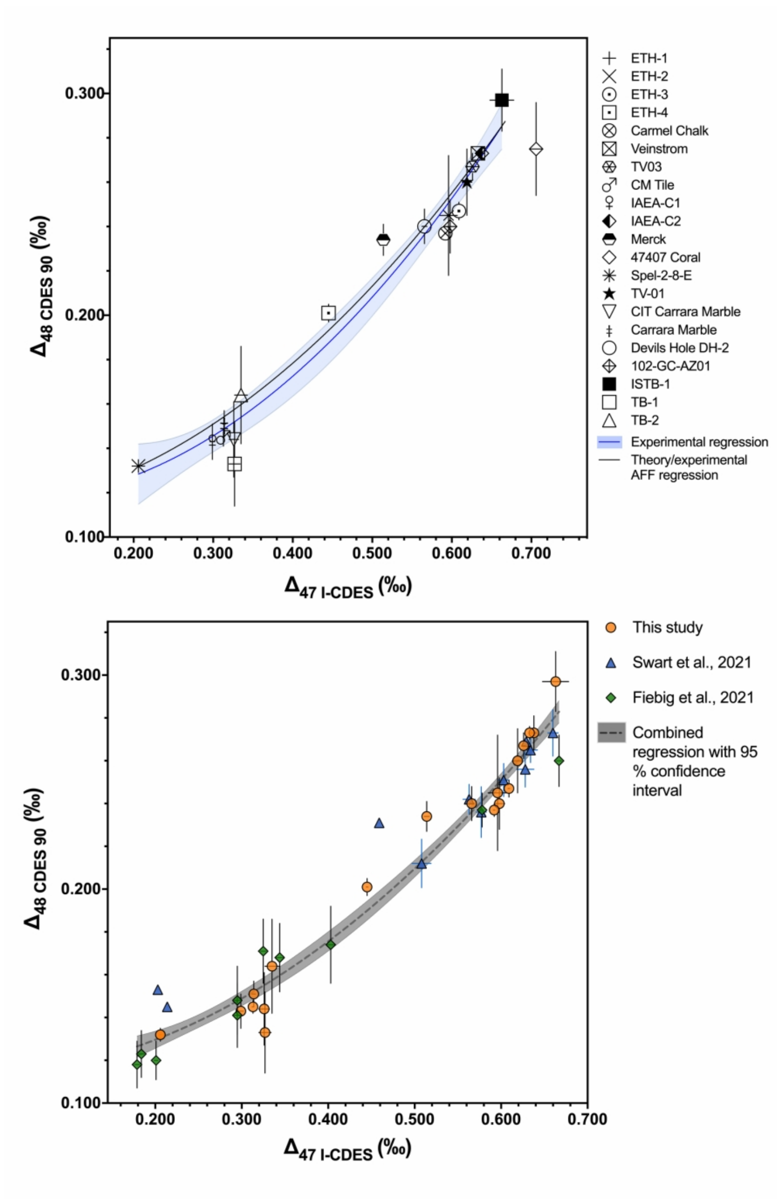

167x256mm (300 x 300 DPI)

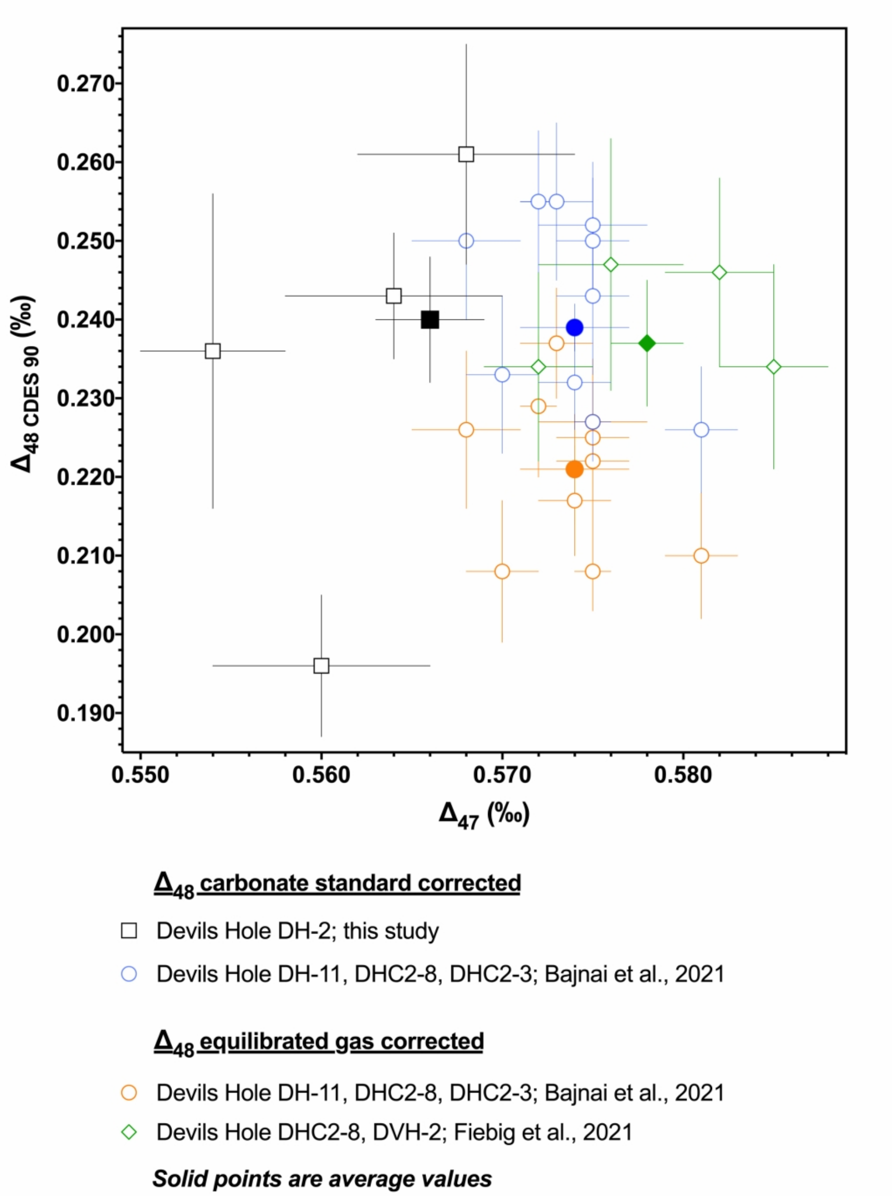

191x252mm (300 x 300 DPI)

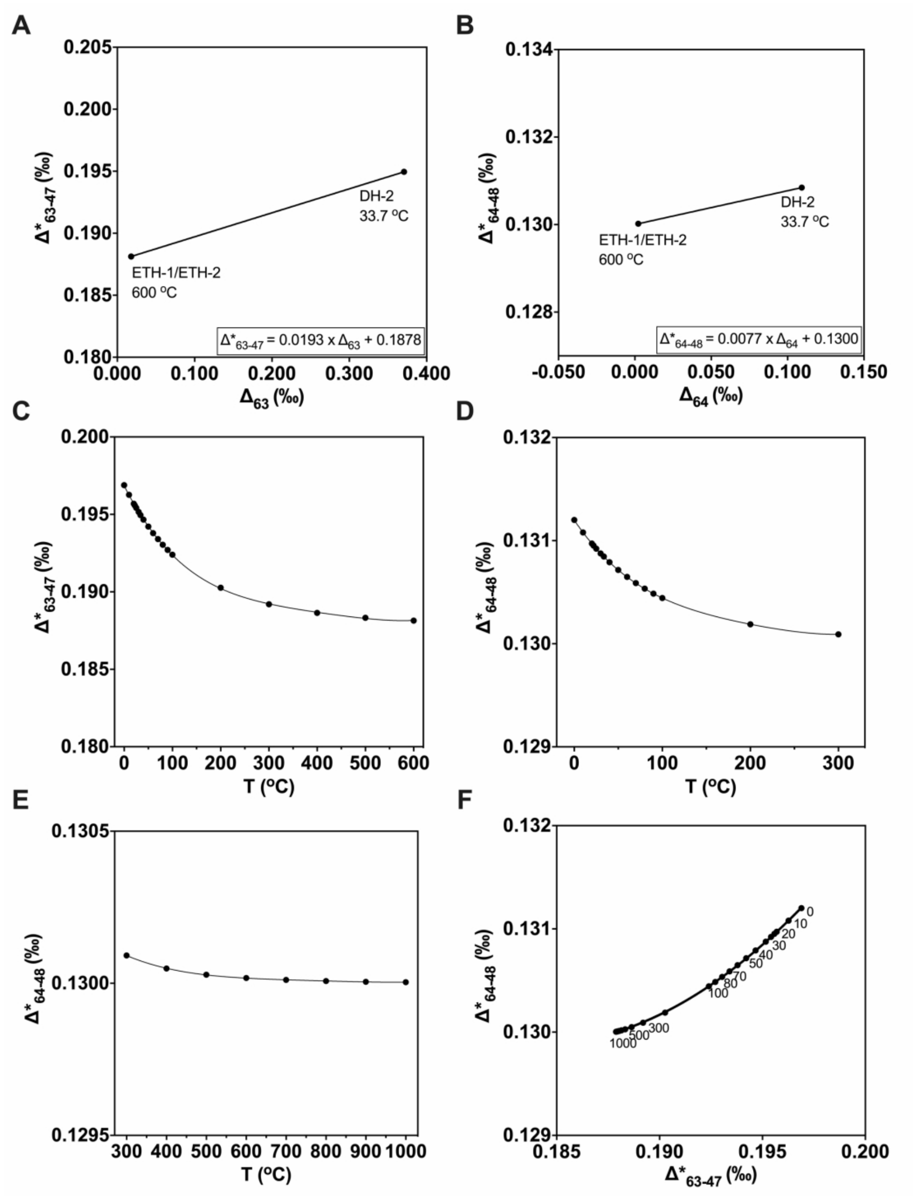

195x254mm (300 x 300 DPI)

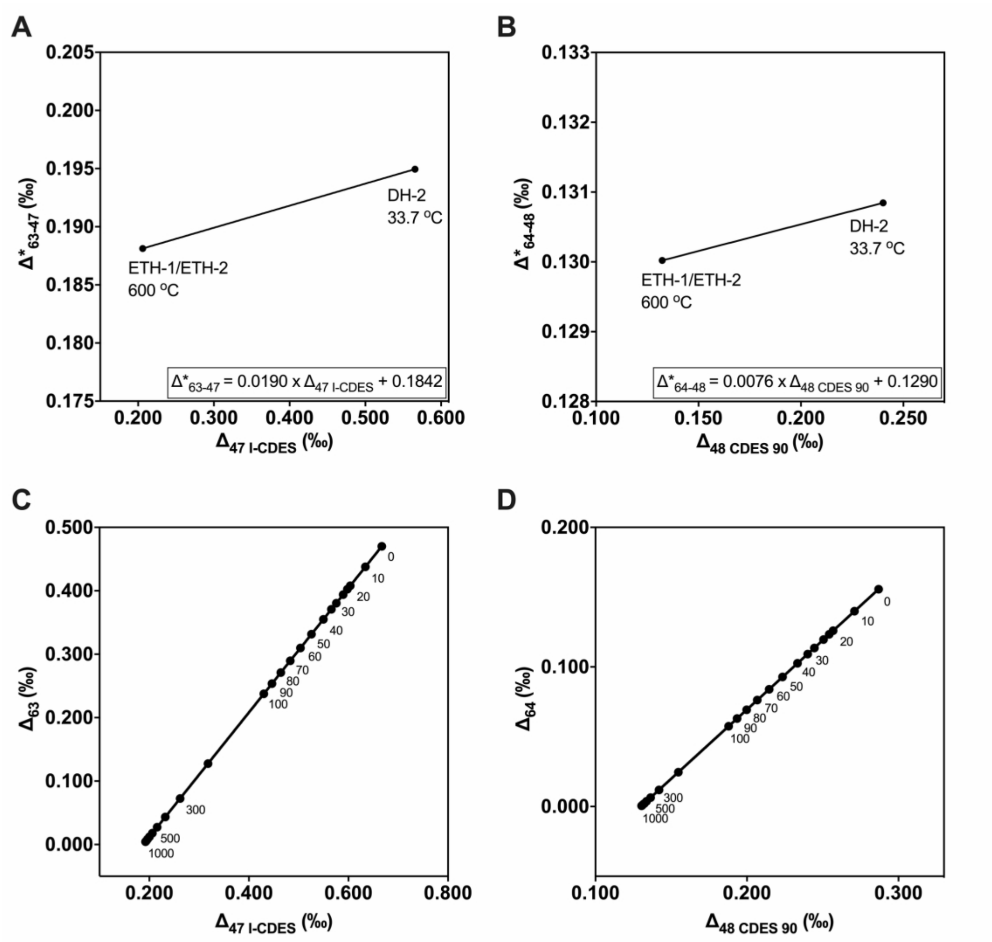

196x186mm (300 x 300 DPI)

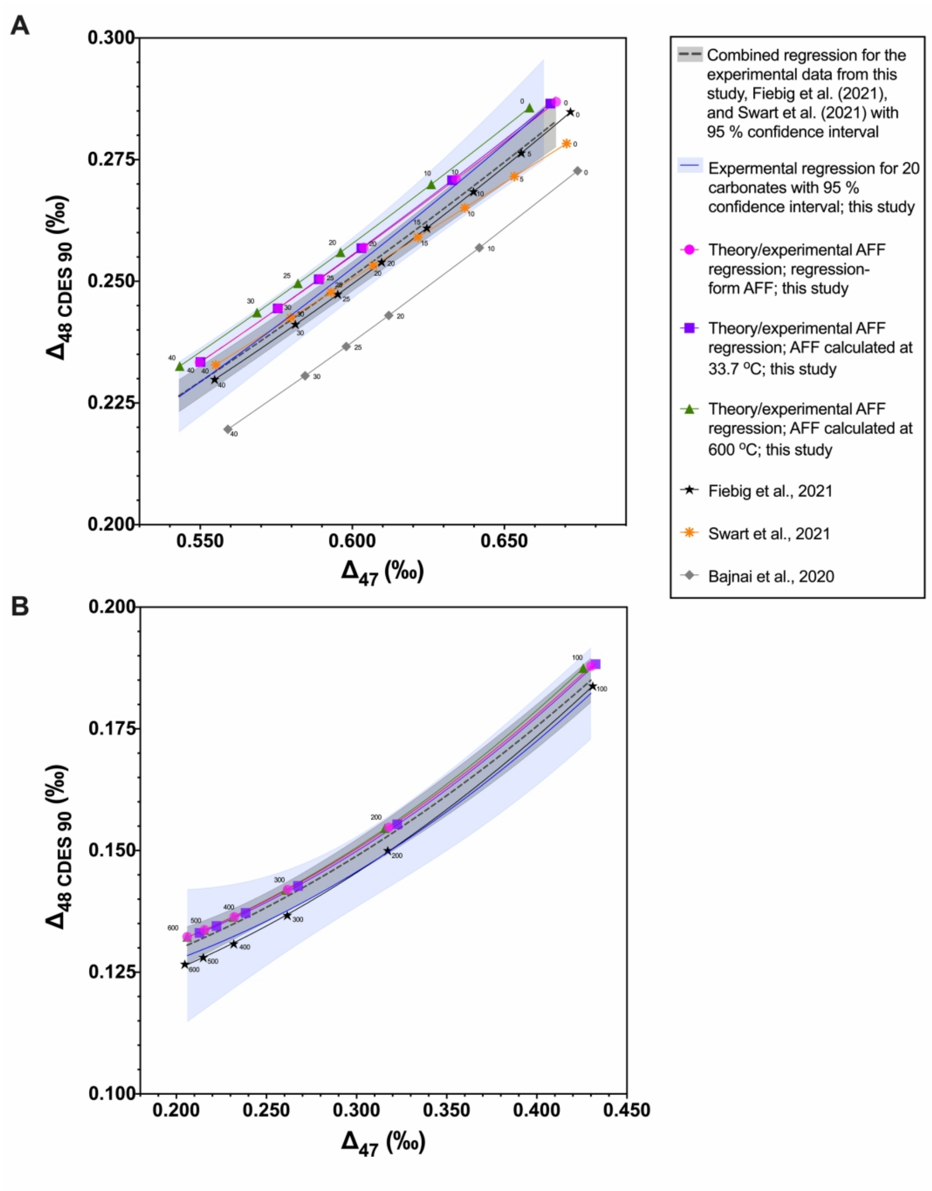

198x252mm (300 x 300 DPI)